Prediction of Statistical Properties of Turbulent Two-Phase Flow Wall Pressure Fluctuations

by

S.M. SAMI and A.A. LAKIS

EP-81-R-39

Technical Report

Ecole Polytechnique

1981

TABLE OF CONTENTS

1. INTRODUCTION

In recent years, the problem of multiphase flow has become of great concern to engineers. Two-phase flow (simultaneous flow of gas or vapour and liquid) is encountered in an increasing number of chemical processing and energy conversion systems.

In particular, the knowledge of the statistical properties and the response of cylindrical shells subjected to pressure field arising from turbulent boundary layer of an internal two-phase flow is of considerable practical interest such as, condensers, heat exchangers, steam generators, evaporators, chemical reactors, petroleum transportation and processing equipment. The more recent applications of vapour-liquid mixtures in the nuclear energy and space technology field have greatly stimulated the demand for a better understanding of pressure field arising from two-phase flow under a variety of conditions.

Mostly cylindrical shells are utilized in either containing or conveying fluids. Concerning the response of cylindrical shells, considerable interest exists in the case where the excitation is transmitted through or arises from the contained fluid [1, 2, 3] . This could take the form of pressure waves transmitted through the fluid or if the fluid is flowing, the excitation could arise from gross pressure pertubation due to disturbance in the flow or from boundary layer perturbations. Vibration caused by these pressure fluctuations may in certain circumstances, cause fatigue failure of the structure involved.

Other effects of coupled fluid-shell motions occur when the fluid is flowing. In connection with the effect of the mean flow on the dynamics of the system, the shell is subjected to centrifugal forces and coriolis-type forces. The former have the effects of diminishing the natural frequencies of the system, while the latter have a damping effect on vibration in cases where one end of the shell is free. Unless dealing with rubber shells, very heavy fluids or very high velocity (1200 m/s), the effects of these forces will be correspondingly small [2, 3] .

Meanwhile, the occurence of pressure fluctuations, due to a two-phase flow, will be determined firstly by the turbulent velocity fluctuations which generate pressure disturbances within the flow and secondly by the manner in which disturbances are propagated through the mixture. Whilst there is little information available concerning the former, due to the difficulty in measuring unsteady velocities, the transmission of fluctuations has been studied analytically in order to determine the drastic reduction in the velocity of propagation of pressure disturbances caused by the introduction of the gas phase and also to determine the strong attenuation of incident disturbances.

The velocity of pressure disturbances has been investigated by Davies [1] amongst others under the assumption that the mixture behaves as a continuum and either achieves thermodynamics equilibrium during the passage of the fluctuations or alternatively that no inter-phase mass transfer occurs. Apparently, for a steam-water mixture, it was

found that this velocity reduced to less than 100 ft/s at a void fraction of 0.5 and at ambient pressure when no mass transfer was considered.

Rushton and Leslie [5] investigated the particular case of flow nozzles and demonstrated that prediction of critical flow can result from assumptions in the mathematical model used. Whilst these appear to be some uncertainties with respect to flows through nozzles, depending upon the way in which the flow is represented mathematically; it may be said that there is more general agreement concerning propagation of disturbances, through homogeneous mixtures as Davies [4] .

However, the influence of inhomogeneities in a real flow situation such as that in a circular pipe considered here cannot immediately be discounted and in this regard the discussion of Rushton and Leslie appears relevant.

Measurements of fluctuating pressures in gas-liquid mixture flows have been reported by Semenov [6] and by Hubbard and Dukler [7] both using air-water mixtures. The regular pressure pulsations set up by slug flows were discussed by Semenov; the predominant frequencies being relatively low. Variations in the reduced amplitude and frequency were related to the flow speed. A maximum in the reduced frequency being found at a void fraction of approximately 0.250. The amplitude of the pressure fluctuations reached a maximum at a much higher void fraction of approximately 0.90. Whilst the overall trends were shown

by these results, the analysis of the fluctuating signals was restricted to the evaluation of the two parameters mentioned. This approach is practicable for sulg flows but not for bubbly flows where it is no longer possible to identify easily a characteristic pulsation wave form. The maximum flow velocity was of the order of 1 m/s.

Hubbard and Dukler carried out experiments at velocities of the order of a few meters per second for slug and annular flows and showed maxima in frequency spectra which could be associated with the flow extending to 6 Hz.

More recently, Davis [8] presented results of a series of measurements of unsteady wall-pressure fluctuations for an upward flow of a vapour-liquid mixture of freon in a circular pipe. His data show the strong attenuation of incident disturbances by the mixture, the generation of pressure fluctuations by the turbulent two-phase mixture and the propagation of pressure disturbances associated with the flow. Davis' investigation was for bubbly flow but unfortunately restricted to very low turbulent flow (mixture velocities less than 5 m/sec).

Apparently, it may be seen throughout this discussion, that only limited information is available concerning the transmission and attenuation of pressure fluctuations by two-phase either vapour-liquid or gas-liquid mixtures in complex flow situations of practical relevance such as flow inside a circular pipe.

The present research was undertaken to increase better understanding of adiabatic two-phase flow concerning wall-pressure fluctuation arising from the passage of such a flow.

This report will be devoted to a qualitative description of the two-phase turbulence mechanism which generates the wall-pressure fluctuations and comprehensive discussion of the sample experimental data conducted in the fully-developed region throughout the loop facility described in an earlier section.

2. TWO-PHASE FLOW LOOP FACILITY

A closed two-phase flow loop system, shown in (figure 1) is designed and constructed to generate fully-developed turbulent two-phase flow. Water was pumped through a centrifugal pump with maximum available pressure head of ninety feet of water. A 15,000 gallon reservoir tank was located adjacent to the pump inlet. The purpose of the reservoir was to provide water storage capacity and to raise the pressure at the pump to prevent cavitation.

The water flow was directed into a closed 2500 gallon pressure vessel, to reduce and suppress the flow irregularities generated by the pump. Then the flow was passed through an air-water mixer (figure 2) where the air was injected to the water flow through 2000 holes havings 3 millimeter diameter distributed homogeneously on the wall of the water conduit. The air-water mixer was employed to ensure homogenous dispersed two-phase flow with different air-water ratios [9] .

The two-phase flow enters a straight run of smooth plastic pipeline (P.V.C.) of eight inches I.D. achieving at the test section a maximum Reynolds' number in the order of 2×10^6 on liquid basis. To assure a fully-developed turbulent two-phase flow, the test section was located 135 diameter downstream.

Factually two-phase pressure drop can be strongly affected by mechanical vibrations transmitted to the pipeline [10]. In order

to eliminate such a build up of the pressure drop, utmost care has been taken to insulate the system from that pulsation by the use of rubber - tubing connection upstream and downstream the pipeline and rubber cushioned machine bolt supports alone the pipeline at 3 feet apart.

Two orifice meters were employed to measure the flow charge for both the water and air flow. Also a Pitot tube assembly associated with hot film anemometry was utilized for predicting the flow velocity of the air-water mixture.

With the flow loop facility it was possible to generate a fully-developed turbulent dispersed two-phase flow in the eight inch diameter working section and gain maximum flow mixture velocity of about 44 m/s. (132 f/s). The corresponding Reynolds' number based on the liquid basis is in the order of 2×10^6.

3. PREDICTION OF PRESSURE GRADIENT IN TWO-PHASE FLOW

In single phase flow, the phase boundaries are defined by the dimensions of the duct in which the flow passes. Two-phase flow is complicated by the fact that the phase boundaries are determined not only by the position of the walls but also by the distribution of the phase in the flow space. Furthermore, this distribution varies with flow rate, fluid properties, conduit size, shape and other factors. The variety of these distributions is called flow regimes, which are separated, intermittent and dispersed flows in horizontal two-phase flow. Until recently, no classification method has proved wholly satisfactory. Most techniques suffered from a heavy dependency on subjective visual observation.

In an attempt to characterize precisely the flow regimes in more quantitative manner, a non-visual approach done by Hubbard and Dukler [7] relied on the fact that the spectral distribution of the wall-pressure fluctuations provided a suitable parameter for flow regime characterization. This method involves the calculation of power spectral density distribution of the wall pressure fluctuations in laminar flows (c.f. figure 3).

Numerous investigators have reported on the difficulty of having reliable pressure drop correlations for two-phase flow regime. A formula derived by Chisholm and Sutherland [11] is considered to predict the pressure changes through turbulent two-phase flow pipeline systems.

It is based on liquid pressure drop as a reference;

$$\frac{\Delta P_{TP}}{\Delta P_L} = 1 + \frac{C}{X} + \frac{1}{X^2} \qquad (1)$$

where

$$X = \frac{1 - Q_1}{Q_1} \left(v_L / v_g\right)^{1/2}, \qquad (2)$$

$$C = \left\{1 + (C_2 - 1)\left(\frac{v_g - v_L}{v_g}\right)^{1/2}\right\}\left\{\left(\frac{v_g}{v_L}\right)^{1/2} + \left(\frac{v_L}{v_g}\right)^{1/2}\right\} \qquad (3)$$

Q_1 is the dryness fraction, i.e. ratio of the mass of the air to the total flow mass; v_g and v_L are the gas and liquid specific volume, respectively. The constanc C_2 is tabulated in reference [11] for various flow conditions and flow parameters. In the present investigation C_2 is equal to one.

Seeking the permissible air-water mixing ratio, equation (3) is plotted in (figure 4) versus volumetric mixing ratio, q. Due to the limited capacity of the available pumps, it is desirable not to exceed an air-water ratio more than q = 0.60, corresponding to X equal to 0.33, where X is the dryness fraction on volume basis.

The pipe exit condition has a very important effect on the flow pattern. Care has been exercised so that such a side effect could be

eliminated. Sekoguchi et al. [12] predicted a formula, to calculate the pipe length L_{CD} from the pipe exit, where the flow pattern could be unaffected,

$$\frac{L_{CD}}{D} = 20 \left(\frac{U_{SGF}}{U_{SWF}}\right)^{0.92} \qquad (4)$$

where

L_{CD} , is the pipe length from exit necessary to avoid exit influence on the flow regime,

D , is pipe diameter

U_{SGF} , is gas superficial velocity, and

U_{SWF} , is liquid superficial velocity.

This formula is valid only for $\left(\frac{V_{GSF}}{V_{LSF}}\right)$ up to 5.

$$\frac{V_{GSF}}{V_{LSF}} \leq 5. \qquad (5)$$

4. PRESSURE FLUCTUATION PICKUPS

Measurements of the wall-pressure fluctuations in turbulent dispersed two-phase flow were conducted using miniature semi-conductor pressure transducers mounted flush with the internal surface of the rigid thick-walled pipe working test section. These pressure transducers are made by Kulite Co. series XCQ-062 with pressure sensitive area of 0.028 inch diameter (0.1772 mm) (c.f. figure 5).

Upon request, Kulite Co. supplied a granted calibration chart for each delivered pressure transducer. Those calibrations have been conducted in their research laboratories due to the lack of such a facility in our laboratories. In addition, characteristic curves have been provided for stability reasons under high frequency excitations.

However examining the calibration curves showed that one of the pressure transducers output signal needed to be amplified and filtered so that its nominal rated output could be achieved. Much care has been paid to that particular pressure transducer through the course of the experiment in order to obtain reliable measurements of the correlation coefficients.

The contact surface of the pressure transducer is covered with Parylene Coating in order to eliminate any misleading disturbances to the transducer performance caused by direct exposure to the air bubbles and the water flow.

The inner surface of the rigid steel pipe was chemically treated to remove all the oxides and mineral deposits and subsequently honed to a smooth wall finish having a tolerance of $\pm$ 0.001 inc. When the plug containing the transducers was mounted flush with the inner surface of the pipe, extreme care was excercised to ensure that there were no protrusions greater than the tolerance limit. Thirteen of the miniature transducers were mounted in the T-shaped slot of a brass plug adaptor which could be inserted in a 1.5 inch diameter hole drilled through the wall of the rigid pipe working section.

The distance between alternate pairs of transducers in the axial and circumferential directions of the cylindrical pipe varied from 0.08 inch for the closest separation to 0.64 inch for the maximum separation. This permitted the wall-pressure cross correlations to be measured over a wide range of transducer separations. (c.f. figure 6).

In order to damp the generated piping noise which may affect the pressure transducer readings, utmost care was taken to ensure that the flow velocities are below the limits of velocity specifications so that piping noise is in order 8-10 db (A) below ambient.

A significant damping of the piping noise was achieved throughout the various parameters discussed (reference [14]), besides employing gradual tapered expanders and reducers as well as bends with ample radii. In addition, gaskets are fitted precisely, minimization of internally well beads and their smoothness are assured.

5. PRESSURE TRANSDUCER ACQUISITION SYSTEM

The signals of each pair of transducers (two channel acquisition system) describing the fluctuations of the wall-pressure field were amplified by Itahco preamplifier model 456-J and passed throughout band pass filter (Itahco, model 4110) to variable gain amplifier (Itahco, model M-55021). Finally, the output signals from the two channel (figure 7) were recorded on a multi-channel tape recorded model UR7671 made by Lyrec Co. A two channel Textronix storage oscilloscope model 564-B was employed to monitor the amplitude-time history of the wall-pressure fluctuations from a given pair of transducers during the course of the experiment.

Because of the turbulent pressure fluctuations are random functions of time and space, it was necessary to define a frequency beyond which amplitudes are almost never large. This defines the frequency requirement of the sensing and amplifying system. For turbulent boundary layer flows, such a frequency might be predicted approximately as (Corcos et al. [13]):

$$f_{max} = 1.6 \left(\frac{U}{r}\right) \text{ cycles/sec.} \qquad (6)$$

where f_{max} is the maximum frequency, U is the characteristic velocity of the stream and r is the pipe radius which is equivalent to the displacement thickness in case of fully-developed flow.

Currently, the Itahco variable band pass filter was necessary to incorporate the recording system so that the extraneous low frequency noise may be eliminated. Due to the amplitude-time history of the dispersed flow was at low amplitude frequency components, the band pass filter was set for a lower cut-off frequency of 25 Hz and an upper frequency to 31.6 KHz.

Factualy, signal to noise ratio depends upon the dynamic pressure of the flow which determines the turbulent pressure level, the characteristic frequency parameter, $\left(\frac{U}{r}\right)$ and the amplification system. As indicated by Corcos [16], it is easier to obtain satisfactory signal to noise ratios in liquid than in gases. That was confirmed in either the presented water flow study or the two-phase flow case. It has been observed over the investigated range of frequency spectra that the water flow shows signal to noise ratio less than that of the two-phase flow.

The low response of the transducer amplifier combination ($\simeq$20 megohms) is defined as the reciprocal of the product of the capacitance and the resistance. However, the input impedance of the preamplifier was about 500 megohms and the capacitance of a transducer and cable connector about 100×10^{-12} farad.

The preamplifier gain was about 15 and the background noise was attenuated to an accepted level. The frequency response was flat to 200 KHz and the preamplifier which is battery powered slow stability throughout the course of investigation.

In practice, it was found necessary to provide further amplification to the signals so that their amplitude-time history could be recorded.

Such an amplification was possible through using the two-matched variable gain Ithaco amplifiers. The total achieved gain was in the order of 25, which permitted the pressure transducer signals to be amplified to a level sufficient for the recording and analysis instrumentation.

6. SPECTRAL ANALYSIS SYSTEM

The statistical properties of the wall pressure fluctuation were performed by direct spectral analysis of the recorded signals from the transducer preamplifier aggregation systems.

An Ithaco 4110 series, variable electronic filters, was used to conduct the spectral analysis in different octave band frequencies. Signal averaging in such octave band frequencies was determined by reading a calibration true RMS voltmeter. In this manner, the RMS and the mean sqare values of the wall pressure fluctuations at various frequencies could be readily determined from a prior knowledge of the transducer sensitivities.

In order to obtain the space-time correlation, the signals from alternate pairs of transducers were recorded directly onto the magnetic tape for a period of about 90 sec., for subsequent analysis using the Honeywell correlator (SAI-43A) and the Fourier Transform-Analyser (FTA-470) fabricated by Honeywell.

The transducer signals were being recorded on two separate channels of the FM tape recorder at a speed of 60 inches per second. This provided a frequency response from Dc to 30 K.c.p.s. A third channel on the tape recorder was utilized for voice recording to identify the transducers and the flow specifications under investigation.

The generation of the pressure fluctuations due to a two-phase flow originates from the turbulent liquid velocity fluctuation, and the gas bubble interaction with the pipewall.

7. INTENSITY OF THE WALL-PRESSURE FLUCTUATIONS

A comparative study of the spectral distributions has been conducted by Hubbard and Dukler [7] for various horizontal two-phase flow patterns, suggested that there is a type of spectra which shows more or less uniform distribution of power over the entire frequency band. This type of spectra corresponds to the visually observed condition where one phase is being dispersed in the second.

They characterize the spectra of such a flow by the degree of concentration of energy in the vicinity of the peak; and the greater the concentration of the energy in a single peak, the more the frequency will coincide with average frequency of the spectra. Their experimental data indicates that the amplitude-time history of the two-phase dispersed flow is characterized by low amplitude and relatively high frequency oscillation (figure 3) with respect to the order of frequency encountered in their laminar flow investigation. Unfortunately neither the work of Hubbard and Dukler [7] nor Davis [8] could be considered as a prediction of the turbulent horizontal two-phase dispersed flow.

Information concerning the intensity of the wall-pressure fluctuations of dispersed two-phase has been obtained through the measurements of the root mean square of the wall-pressure fluctuations and the power spectral density. These measurements have been conducted over center band frequency ranging from 56.23 to 891.24 Hz and at various center-line mixture velocities varying between 51.8 and 146.06 ft/sec.

Extensive care has been exercised to diminish the extraneous background noise in the test section which could be detected by the wall-mounted pressure transducers. It was possible to achieve such a goal because of the various precautions considered in constructing the loop facility. (c.f. section 2), and the low gain of the variable gain amplifier.

However, it was necessary to establish the lower limiting frequency so that the definite interference of the background noise with the signal produced by the local boundary layer turbulences could be eliminated. Apparently, it has been noticed from the power spectra measurements that the background noise was detectable at frequencies less than 30 Hz. Therefore, recordings of the mean square pressure in 1/3 octave bands were performed at frequencies higher than 30 Hz, so that the overall RMS signal may arise only form the turbulent boundary layer pressure fluctuations.

Preliminary tests showed that the two-phase flow wall-pressure fluctuation seems to be characterized by lower amplitude frequency spectra rather than those observed by water flow. Such a behavior may be attributed to the damping effects occured by the presence of the air bubbles.

8. RMS WALL-PRESSURE FLUCTUATIONS

Measurements of the RMS pressure fluctuations induced by two-phase flow have been carried out in octave frequency bands for various center-line pipe flow velocities at Reynold's number of 0.819×10^6 to 2.0874×10^6 on liquid basis. Such a variation inflow velocities was commensurated with the available pump and compressor capacities.

Initial series of experiments have been performed in order to investigate the extraneous contribution of the transducer vibrations and the electronic noise to the output signal of the transducer. There are three extraneous sources contributing to the transducer output signals, they are the spurious signals caused by transducer vibrations, the electronic noise in the amplification system and the background noise at low frequency.

Tests showed that the vibration signals and electronic noise in the amplifier were less than 0.5 percent of the mean square pressure and currently their effects on the spectral density measurements were negligible. That establishes clearly the active role, which the background noise could play.

In connection, the background noise was almost eliminated over the range tested (25 HZ - 31.5 KHZ) and the output signals of the

transducers were generated originally by the boundary layer dominated by the two-phase dispersed flow.

The root mean square wall-pressure fluctuation has been measured over broad variety of flow speeds. Samples of such measurements are shown in (figure 8). It appears from such a figure that the value of $\sqrt{\overline{P^2}}$ increases as the center-line flow velocity increases, such a behavior has been noticed by various investigators for single phase flow.

The effect of the volumetric mixing ratio on the root mean square of the wall-pressure fluctuations has been demonstrated in (figure 9), which shows the dependency of the $\sqrt{\overline{P^2}}$ value upon the volumetric mixing ratio, q. As the volumetric mixing ratio increases the $\sqrt{\overline{P^2}}$ diminishes. That is attributed to the reducing of the mixture velocities which is a resultant of the interaction of interia, friction, surface tension and turbulent dynamic forces. These forces dominate the dynamic pressure force acting on the pipe wall.

The pressure coefficient has been evaluated over wide ranges of the mixing ratio on volume basis from 0.174 to 0.60 and plotted against the Reynold's number in (figure 10). It seems from such a plot that the pressure coefficient is independent of Reynold's number and might be expressed as:

$$\frac{\sqrt{\overline{P^2}}}{1/2\ \rho_m\ U^2_{m_{CL}}} \simeq 0.002 \qquad (7)$$

where,

$\sqrt{\overline{P^2}}$, represents the whole root mean square value of the wall-pressure fluctuations,

ρ_m , is the mixture density, and

$U_{m_{\mathcal{L}}}$, is the center-line mixture velocity.

In fact, such a correlation proved to agree with the results reported for single phase flow, regarding the independence of pressure coefficient upon the Reynold's number. With respect to the correction factor for the loss of resolution, no attempt has been made in the two-phase flow measurements to account for such a loss (c.f. figure 3). No available data for comparison were reported in the literature.

9. POWER SPECTRA MEASUREMENTS

It is important to mention that increasing the void fraction results in a diminution of the mixture velocity (c.f. reference [14]) and the intensity of the turbulence of the pressure fluctuations. To illuminate that (figure 11) the power spectra has been depicted versus the Strouhal's number. Examining this figure spread out that the power spectra might be correlated with the frequency dimensionless parameter [2] as follows:

$$\frac{\Phi_p(f)}{\rho_m^2 \, U_{m_{CL}}^3 \, .D} = k_1 \, e^{-k_2 \, S} \qquad (8)$$

where,

S , the Strouhal's number equal to $\frac{f_o \, .D}{U_{m_{CL}}}$,

k_1 , 2.28×10^{-6}

k_2 , 87.8583×10^{-3}

ρ_m , is the mixture density

$U_{m_{CL}}$, represents the center-line mixture velocity,

D , is the pipe diameter and f_o is the center frequency band.

Such a correlation showed that the normalized power spectral density is independent of the volumetric mixing ratio and consequently the center-line flow velocities in the special case of fully-developed turbulent dispersed two-phase flow.

Moreover, the proposed correlation proves to be similar to those of Bakewell et al., Clinch and other investigations reported in the literature. Meanwhile, this correlation seems to be universal for all the fluid and gases.

In a qualitative sense, the normalized power spectra distribution shown in (figure 11) differs from those of single phase, where it was possible to detect the low Strouhal's numbers. The similarity of both the two-phase dispersed flow spectra and that of the single phase exposes the homogeneity of the experienced two-phase flow. The authors would like to point out that, such a correlation might not be generalized for the other flow patterns of the two-phase flow. No attempt has been made to compare the presented results due to the lack of such a correlation in the literature.

10. SPATIAL CORRELATIONS

In order to predict the mean square response of a cylindrical shell induced by turbulent two-phase dispersed flow, (c.f. reference [14]) it is necessary to determine the spatial correlation in the lateral and axial directions of the internal pressure field. Measurements of such spatial correlations have been conducted over broad variety of mixing ratios on volume basis and mixture flow velocities. Such correlations have been obtained by replaying back the recorded two-phase signals through octave band filters and processing through a correlator and Fourier transform analyzer. The narrow band spatial correlations were conducted over different center band frequencies ranging from 56.223 to 891.24 Hz, and they have been examined at broad varieties of flow velocities from 51.80 to 146.02 ft/sec.

10.1 Lateral correlations

Samples of the experimental data representing the lateral correlations have been displayed through (figure 12) (c.f. figures 8.5 to 8.12, reference [14]) versus the transducers separation in the circumferential direction, η (c.f. reference [14]) for wide variety of mixture flow velocities. In addition, for a given mixture flow velocity, various sets of curves were plotted for different center frequency bands. Examining these curves shows that the lateral correlations are characterized by having an exponential function diminishing with the augmentation

of transducers separation. Such a behavior has been observed by various investigators for the case of single phase flow, which proves the similarity of the mixture.

On the other hand, it may be observed that increasing the transducer separations in the lateral direction will result in lessening the circumferential spatial correlation to approximately a certain value of the transducer separation equals to 0.30 inch, then the circumferential spatial correlation seems to be independent of the spatial separation. Such phenomenon was observed in almost all the gas and liquid investigations and it was found that the maximum separation whereas the lateral correlation is independent of the transducers separation varies with the type of flow. In addition, it appears from the obtained data (reference [14]), that for a given transducer separation, the amplitude of the spatial lateral correlations seem to be reduced as the center band frequency increases. However for a given spectral central frequency band, the spatial circumferential correlation coefficient augments in amplitude as the mixing air-water ratio dwindles. That behavior could be interpreted as the void fraction decreases, the interfacial structure forces acting on the bubbles reduces. That results in increasing the dynamic pressure forces which cause the correlation coefficient amplitude to raise up.

Currently, the main objective of the presented study is to predict the spatial lateral correlation in terms of the non-dimensional

Strouhal's number. Therefore, the samples of the correlation coefficient have been plotted versus Strouhal's number for various values of the mixing ratio on volume basis in (figure 13).

Such a figure demonstrates that the correlation coefficient in the circumferential direction could be expressed in terms of the Strouhal's numbers in a similar form to Bakewell et al. [15] but with different constants, $\bar{a}$, and $\bar{b}$, which are dependent upon air-water mixing ratio, q, and the inlet conditions;

$$\Psi_p(0, \eta, 0) = (1 + \bar{a}\, S_\eta^2)^{-1} \quad (2 - e^{\bar{b}\, S_\eta^2})^{-1} \qquad (9)$$

where,

$\Psi_p(0, \eta, 0)$, represents the correlation coefficient in the lateral direction as a function of the Strouhal's number,

$S\eta = \frac{\eta \cdot f_o}{U_{m_{\mathcal{L}}}}$, with f_o, as the central band frequency, D, is the pipe diameter, $U_{m_{\mathcal{L}}}$ is the mixture center-line velocity, and, q, is the air-water mixing ratio.

In order to identify the functional dependence of $\bar{a}$ and $\bar{b}$ upon the air-water mixing ratio, q, various values of $\bar{a}$ and $\bar{b}$, have been plotted versus q, in (figure 14).

It appears that $\bar{a}$ and $\bar{b}$ have a linear dependence upon the air-water mixing ratio q, on volume basis and they might be expressed as follows;

$$\bar{a} = 46.557 - 40.1516 \cdot q \qquad (10)$$

$$\bar{b} = -36.0231 + 58.747651 \cdot q \qquad (11)$$

To this end the spatial correlation in the circumferential direction has been predicted in terms of both the non-dimensional frequency parameter and the air-water mixing ratio on volume basis. No other correlations were available for comparison. It should be noted that the presented correlation may not be applicable to other two-phase flow patterns.

Moreover, measurements of the spatial correlation in the lateral direction showed no convection in the circumferential direction, therefore, no attempt has been made to investigate the time delay effects upon the spatial lateral correlation coefficient.

10.2 Axial correlation function

The measured data of the space-time correlation coefficient in the axial direction have been examined at wide variety of two-phase flow speeds and were analyzed at different narrow band frequencies, so that the mean square response could be exclusively determined.

Samples of those experimental data have been displayed versus the axial transducers separation, ξ, through (figures 15 and 16 and reference [14]). These figures indicate that the axial correlation coefficients are featured by an exponential damping cosine function. Moreover, the axial spatial correlation coefficient as expressed in terms of the transducers axial separation, is well distinguished in the region of higher mixing ratios of air and water, and particularly at higher frequency spectra as shown in (figure 15). In fact, such a behavior is attributed to the enlargement of the air bubble sizes, that results in increasing both the inertia forces and the friction forces. These forces together with the turbulent dynamic forces will diminish the pressure force applied on the wall, and consequently the axial correlation coefficient amplitudes.

To investigate the effects of varying the air-water mixing ratio on the correlation coefficients, different samples (c.f. figures 8.5 to 8.22, reference [14]) have been examined for either a given spectral frequency or a transducers separation. It has been observed that at higher air-water mixing ratio the axial correlation coefficient diminishes.

Of particular interest is the effects of the pressure disturbance frequency spectra on the correlation coefficient. (c.f. figure 15). From such a figure it has been remarked that for a fixed air-water mixing ratio. The frequency spectra plays an important role indetermining.

the values of the correlation coefficient amplitude and an increase in the pressure disturbance frequency will result in reducing the value of the correlation amplitude.

Seeking a general empirical correlation, to express the wall-pressure correlation coefficient in the axial direction in terms of the non-dimensional frequency number, (figure 16) has been constructed by plotting the correlation coefficient versus the Strouhal's number for various values of the mixing ratio on volume basis.

The graphical representation shows that the spatial correlation coefficient in the flow direction might be expressed as a function of both the Strouhal's number and the air-water mixing ratio as follows:

$$\Psi_p(\xi, 0, 0) = \cos \pi \frac{S\xi}{\bar{c}} \; e^{\bar{d}} \; S_\xi^2 \qquad (12)$$

where,

$\Psi_p(\xi, 0, 0)$, is the axial correlation coefficient,

S_ξ, represents the Strouhal's number defined as $\xi, fo/U_{m_{\ell}}$, with ξ, is the transducer axial separations, and f_o represents the spectral analysis frequency.

It is worthwhile to point out that such a correlation function is similar to the form obtained by Bakewell et al. [15] for single phase

flow. The constants $\bar{c}$ and $\bar{d}$, are mixing ratio dependents as previously found in the case of the lateral spatial correlation.

Furthermore, the variables of the correlation have been calculated for each value of the air-water mixing ratios and plotted function of q, in (figures 17 and 18), respectively.

The variable $\bar{c}$, might be expressed as straight line relation with q, for the best fit:

$$\bar{c} = 0.517908 - 0.30355 \cdot q \qquad (13)$$

with, q as the air-water mixing ratio on volume basis.

Also, the values of $\bar{d}$ have been examined over the broad range of air-water mixing ratio q, the outcome shows that:

$$\bar{d} = -0.62776 - 0.90962 \cdot q \qquad (14)$$

where q represents the volumetric mixing ratio. No available correlations for two-phase dispersed flow have been cited in the literature.

Unfortunately, due to either the high flow mixture velocities or the limited number of axial transducers separation located in T-slot employed for wall-pressure fluctuation measurement, no higher Strouhal's numbers could

be obtained through the course of the investigation. In addition, the low amplitude frequency spectra of the two-phase dispersed flow was a crucial factor in extending the wall-pressure correlation coefficient to the higher Strouhal's numbers.

Furthermore, as given by Bakewell et al. [15], the empirical expressions for the axial and lateral space-time correlation functions should satisfy the following conditions:

$$\Psi_p(0,0,0) = 1.0 \tag{15}$$

$$\lim_{\xi \to \alpha} \Psi_p(\xi,0,0) = 0 \tag{16}$$

$$\lim_{\eta \to \alpha} \Psi_p(0,\eta,0) = 0 \tag{17}$$

$$\left.\frac{\partial \Psi p(\xi,0,0)}{\partial \xi}\right|_{\xi = 0} = \left.\frac{\partial \Psi p(0,\eta,0)}{\partial \eta}\right|_{\eta = 0} \tag{18}$$

$$\Psi_p(\xi,0,0) = \Psi_p(-\xi,0,0) \tag{19}$$

$$\Psi_p(0,\eta,0) = \Psi_p(0,-\eta,0) \tag{20}$$

Such properties are valid for the spatial, lateral and axial correlation for all the values of the air-water mixing ratios, and are limited to the special case of turbulent dispersed two-phase flow.

11. PREDICTION OF WALL-PRESSURE CONVECTIONS

To predict the convection of the wall-pressure fluctuation in the axial direction, the recorded transducer signals of turbulent two-phase flow have been replayed through the octave filters to the correlator whereas, a broad range of time delay between the two recorded signals could be performed. Samples of these data have been plotted in (figure 19) (c.f. figures 8.26 to 8.50, reference [14]) covering the whole investigated range of both flow mixture velocities and center band frequencies.

Through examining these figures, it might be observed that the general features of the correlation-time delay curves are similar to those obtained for single phase turbulent flow [14]. However, whereas the two-phase dispersed flow correlation time delay curves exhibit broader, flatter peaks with increasing transducers separation, and the shape of each correlation curve is governed by the frequency.

Furthermore, at higher mixing ratios on volume basis, the high frequency correlations are characterized by sharp narrow curves and the low frequencies by broader correlation curves.

It has also been remarked through the course of the correlation time delay investigation that the correlation maxima diminish as the transducers separation increases. That is attributed to the shearing forces, the air bubble generated forces as inertia and friction, and

surface tension forces which resist the two-phase flow as convected downstream.

In addition, it was found that at various spectral frequency the space correlation-time delay curves would have a similar behavior to those obtained through the single phase flow investigation such as the maxima of the correlation coefficient decreases at higher spectral frequency analysis.

The propagation of pressure disturbances along the fully-developed turbulent region have been exclusively discussed in (reference [14], c.f. figures 3.25 to 8.50). Importantly, a peak may be observed in the cross correlation coefficient showing that there is a propagation of the wall-pressure pattern from upstream to downstream. A convection mixture velocity may be defined in terms of time delay for a maximum correlation, τ_o, and the separation, $\Delta\xi$, and could be determined similarly to the single phase flow.

A display of samples of the convection velocity obtained from the space time correlation function and the average air-mixing ratio has been shown in (figure 20).

It may be seen that the convection velocity varies between 1.14 to 1.271 times the mixture center-line velocity. It is evident from these results that the low void fraction data do appear to have on the average lower values of the normalized convection velocity,

$\left(Uc/Um_{\ell}\right)$, the average value of $\left(\frac{Uc}{Um_{\ell}}\right)$ is 1.20 over all the obtained results and the spread being approximately ± 5.16%. To investigate the Reynold's number effects upon the convection velocity (figure 21) has been constructed. Examining this figure shows that the ratio $\left(\frac{U_c}{U_{m_{\ell}}}\right)$ is almost independent of Reynold's number and;

$$\left(\frac{U_c}{U_{m_{\ell}}}\right) \simeq 1.140 \qquad (21)$$

These results indicate that the pressure disturbances would be associated with the passage of the bubble structures and their wakes along the pipe in the flow direction. It is believed that the large scale eddies associated with large voids will be swept with higher rates of convection than those of small voids with small scale eddies.

To study the effects of varying the center frequency upon the ratio of the convection velocity to the center line velocity (figure 22) has been depicted. It is apparent that the ratio, $\left(\frac{U_c}{U_{m_{\ell}}}\right)$, decreases slightly from 1.3 to 1.10 at 890 Hz. This decrescence of $\left(\frac{U_c}{Um_{\ell}}\right)$, with frequency is in good agreement with those results of others, notably Bakewell et al. [16] and Clinch [17] for single phase flow.

Similarly to the single phase, it is suggested that the large voids and large scale eddies are associated with low frequency spectra and both small voids and small scale eddies are converted upstream with high

frequencies. No other interpretation was possible. In general, the two-phase flow data seem to have higher ratios of $\left(\frac{U_c}{U_{m_G}}\right)$ than those of single phase flow. That is mainly attributed to both the higher velocities of gas bubbles than eddies and the attraction caused by the bubbles turbulence wakes upon the eddies.

It has been shown experimentally for single phase flow by Corcos et al. [13], Bull and Willis [18] and Clinch [17] that the turbulent wall-pressure field is convected in the flow direction and its space time correlation function could be expressed as;

$$\Psi_p(\xi,0,\tau) = A_c \cos f_o \left(\tau - \frac{\Delta\xi}{U_c}\right) \qquad (22)$$

where,

U_c , is the convection velocity of the turbulent disturbance in spectral frequency, f_o, and

$\Delta\xi$, the spatial separation in the flow direction,

A_c , the amplitude of the cosine function which represents the envelope of the peaks of the normalized correlation.

In addition, it was reported by Harrison [19] and Bull and Willis [18] that such an amplitude has a unique function of the Strouhal's number, $S_\xi = \frac{\Delta\xi, f_o.}{U_c}$

In the present analysis, an attempt will be made to predict that unique function in the special case of the turbulent dispersed two-phase flow. Therefore, (figure 23) has been constructed to display samples of the amplitudes of the normalized axial spatial correlation as a function of the Strouhal's number, S_ξ , and the volumetric mixing ratio, q. It could be easily shown that the amplitude A_c might be determined in terms of the Strouhal's number, S_ξ , as,

$$A_c = 0.8221\, e^{-1.3315} \cdot S_\xi \qquad (23)$$

where,

A_c, is the amplitude of the cosine function representing the envelope of the peaks of the normalized axial correlation,

S_ξ, is the Strouhal's number and is defined as, $\frac{\Delta\xi \cdot f_{o.}}{U_c}$

12. ESTIMATION OF THE MICROSCALES OF TURBULENCE

This section will discuss the prediction of the microscales of turbulent two-phase flow. The approach applied in (reference [14]), to determine the lateral and axial microscales will be adopted for this study.

Through experimentations of the two-phase dispersed flow, it has been observed that the lateral and axial correlations seem to have functional dependence upon the volumetric mixing ratio of the two-phases, therefore, it was suggested to investigate the circumferential and axial microscales over either a wide range of mixing velocities or various center band frequencies.

(Figures 24 and 25) have been constructed to display the microscales in lateral and axial directions over different mixture velocities. It appears from such figures that larger microscales are associated with low frequency spectra and higher velocities. The influence of the inlet conditions and the mixing ratio of the two-phase could be demonstrated through the strong relationship between mixing ratio and mixture velocity (c.f. reference [14]).

In order to predict the relationship between the axial and lateral microscales, (figure 26) has been created, whereas, either the axial or the circumferential microscales have been displayed versus the center band frequencies.

It could be noticed through such data and others tabulated in (reference [14]), that the ratio of the circumferential microscales to the axial ones has an average value of:

$$\frac{\lambda_{mn}}{\lambda_{m\xi}} \simeq 0.21415 \qquad (24)$$

In a qualitative sense, the ratio of microscales in axial and lateral direction is in agreement to those observed in single phase flow. Moreover the ratio of $\left(\frac{\lambda_{mn}}{\lambda_{m\xi}}\right)$ shows less values than those of single phase flow which is attributed to the precence of the air bubble and their highly convection in the axial direction more than that in the lateral direction.

In addition, it is also believed, that the higher ratio of the convection velocity to the center-line velocity has a significant effect on such microscale ratios.

13. BROAD-BAND SPACE-TIME CORRELATIONS

The measurement of the broad-band space-time correlations has been obtained similarly to the narrow band space-time correlation by playing back the recorded signals for a given pair of pressure transducers through the variable time delay correlator. A description of the instrumentation has been demonstrated in (section 6).

Broad-band space-time correlations of the wall-pressure field in the axial flow direction have been presented in through (figure 27 to 29), whereas the cross-correlation coefficient is displayed as a function of the time delay. Various separations, i.e. distances between transducers, have also been shown in such figures. It might be observed from presented results that the main characteristics of such correlations are similar to the narrow band correlation predicted in previously. However, the broad-band correlation of the dispersed two-phase flow seems to exhibit broader, flatter peaks. Similarly to narrow band correlations, the amplitude of the correlation coefficient maxima decrease rapidly with increasing transducer separation.

In addition, to predict the influence of varying the mixture velocity on the broad-band correlation, (figure 27) has been constructed. Examining the plotted results shows that at higher mixture, velocities, the amplitude of the correlation coefficient drastically increases which has been interpreted in an earlier stage of this report.

A comparison is shown through (figures 27 to 29) so that the order of the axial to the lateral space-time correlations might be demonstrated. It could be noticed through the data depicted in these figures that the correlation coefficient in the axial direction seems to have higher values than those of the correlation coefficient in the circumferential direction. This suggests that the wall-pressure field is coherent over much greater distances in the flow direction than in the lateral direction.

In addition, (figures 28 and 29) have been constructed to expose the influence of varying the volumetric mixing ratios. It appears from these figures that the broad-band correlation coefficient amplitude - separation diagram have similar characteristics to those predicted in narrow band frequencies, whereas reducing the volumetric mixing ratio would result in increasing the amplitude of the correlation coefficients.

Finally, (figure 30) has been constructed to demonstrate the broad-band convection ratio, $\left(\frac{U_c}{U_{m_{QL}}}\right)$, reliance on the mixing ratio on volume basis, q. It could be easily shown that the broad-band convection ratio increases slightly as the volumetric mixing ratio increases. On the average the ratio appears to be:

$$\frac{U_c}{U_{m_{QL}}} \simeq 1.115 \qquad (25)$$

The deviation is in the order of 2.31 per cent from the average value. Such an observation has been interpreted earlierly.

To this end, an analysis of certain statistical properties of wall-pressure fluctuations has been accomplished and though properties have been investigated and related to the volumetric mixing ratio which is a crucial parameter from the point of view of the parctical experience in the two-phase flow applications.

14. CONCLUSIONS

In the present work attention has been directed towards the analysis and measurement of the wall-pressure field over a wide variety of both the turbulent flow conditions and mixing ratios on volume basis of the two-phase flow.

Our contribution to the wall-pressure fluctuations in the special case of dispersed turbulent two-phase flow, could be summarized as follows:

1- The intensity of the wall-pressure fluctuations has been studied over a wide range of highly loaded two-phase flow system, such a study demonstrates that the RMS of the two-phase flow seems to have values less than those single phase flow (water or air).

2- The RMS values appear to diminish as the mixing ratio increases.

3- The pressure coefficient showed over a broad range of mixing ratios that it is independent of the Reynold's number and its value is less than that obtained for water flows.

4- The normalized power spectra of the two-phase flow pressure field may be expressed as a function of Strouhal's number based on pipe diameter length and is similar in shape to those of water flows. It is important to mention that the low frequency numbers covers more range than that of single phase flow.

5- The lateral spatial correlation is expressed in terms of circumferential Strouhal's number. The constants of that function have a linear dependence upon the volumetric mixing ratios.

6- Similarly the streamwise spatial correlations have been determined, as a function of the axial Strouhal's number with an exponential cosine damping form. Furthermore, the constants of that correlation could be correlated linearly with the mixing ratios on volume basis.

7- The wall-pressure field convection showed an increase at higher two-phase flow mixing ratios on volume basis. The ratio of convection velocity to center-line velocity diminishes at higher spectral frequency which is qualitatively similar to single phase flows.

8- A useful correlation has been developed to predict the correlation amplitude in terms of the Strouhal's number and time delay.

9- The lateral microscale of turbulence seems to be approximately five times that of axial direction. Apparently, both the microscale of turbulence decrease with increasing the frequency spectra.

15. REFERENCES

[1] Lakis, A.A., «Effects of Fluid Pressures on the Vibration Characteristics of Cylindrical Vessels», Proceeding of the 2nd Int. Conf. on Pressure Surges, Sept. 1976.

[2] Lakis, A.A. and Paidoussis, M.P., «Prediction of the Response of a Cylindrical Shell to Arbitrary Boundary Layer Induced Random Pressure Field», J. Sound and Vibration, Vol. 25, pp. 1-27, 1972.

[3] White, F.M., «A Unified Theory of Turbulent Wall-Pressure Fluctuations», U.S. Navy Underwater Sound Lab., Report No. 629, 1964

[4] Davies, A.L., «The Speed of Sound in Mixtures of Water and Steam», Proceedings of EURATOM Symposium on Two-Phase Flow Dynamics, Eindhoven, pp. 625-638.

[5] Rushton, E. and Leslie, D.C., «A Reappraisal of Silver's Model for a Satured Water Flow Through Nozzles», Br. Chem. Engng. 14, pp. 319-323, 1964.

[6] Semenov, N.I., «Pressure Pulsations During the Flow of Gas-Liquid Mixtures in Pipes», United States Atomic Energy Commission Technical Report 4496 (translated from U.S.S.R. Academy of Sciences Publications), 1959.

[7] Hubbard, M.G. and Dukler, A.E., «The Characterization of Flow Regimes for Horizontal Two-Phase Flow», Proceedings of the 1966 Heat Transfer and Fluid Mechanics Institute, Stanford, 1966.

[8] Davis, M.R., «Pressure Fluctuations in a Vapour-Liquid Mixture Flow», Int. J. Heat Mass Transfer, Vol. 15, No. 11, p. 2048, 1973

[9] Sami, Mohamed, S., «Terminal Velocity of Bubble Trains, Effect of Bubble Size and Frequency», M.Sc.A. Thesis, Cairo University, Cairo, Egypt, 1976.

[10] Petrick, M. and Swanson, B.S., «Expansion and Contraction of an Air-Water Mixture in Vertical Flow», A.I.Ch.E.J. 5-4, p. 440, 1959.

[11] Chisholm, D. and Sutherland, L.A., «Prediction of Pressure Gradients in Pipeline Systems During Two-Phase Flow», Proc. Instn. Mech. Engrs., Vol. 184, p. 24, 1970.

[12] Sekoguchi, K., Sato, Y. and Kariyasaki, A., «The Influences of Mixers, Bends, and Exit Sections on Horizontal Two-Phase Flow», Trans. JSME, 33-260, p. 1810, 1973-11.

[13] Corcos, G.M., Cuthbert, J.W. and Von Winkle, W.A., «On the Measurement of Turbulent Pressure Fluctuations with a Transducer of Finite Size», University of California, Institute of Engineering Research, Series 82, Issue No. 2, 1959.

[14] Sami, S.M., «Prediction of Velocity and Wall-Pressure Fluctuations of Turbulent Two-Phase Dispersed Flow», Ph.D. Thesis, University of Montreal, Ecole Polytechnique, 1981.

[15] Bakewell, H.P. Jr., Carey, G.F., Libuha, J.J., Schloemer, H.H. and Von Winkle, W.A., «Wall-Pressure Correlation in Turbulent Pipe Flow», U.S.L. Report No. 559, 1962.

[16] Corcos, G.M., «On the Resolution of Pressure in Turbulence», J. Acoustic Soc. Am., 35, p. 192, 1963.

[17] Clinch, J.M., «Study of Vibrations Induced in Thin-Walled Pipes Under Varying Flow Conditions», Contract No. 20325, NASA, 1967.

[18] Bull, M.K. and Willis, J.L., «Some Results of Experimental Investigations of the Surface Pressure Field Due to a Turbulent Boundary Layer», University of Southampton, A.A.S.U. Report No. 199, 1961.

[19] Harrison, M., «Pressure Fluctuations on the Wall Adjacent to a Turbulent Boundary Layer», David Taylor Model Basin, Report No. 1260, 1958.

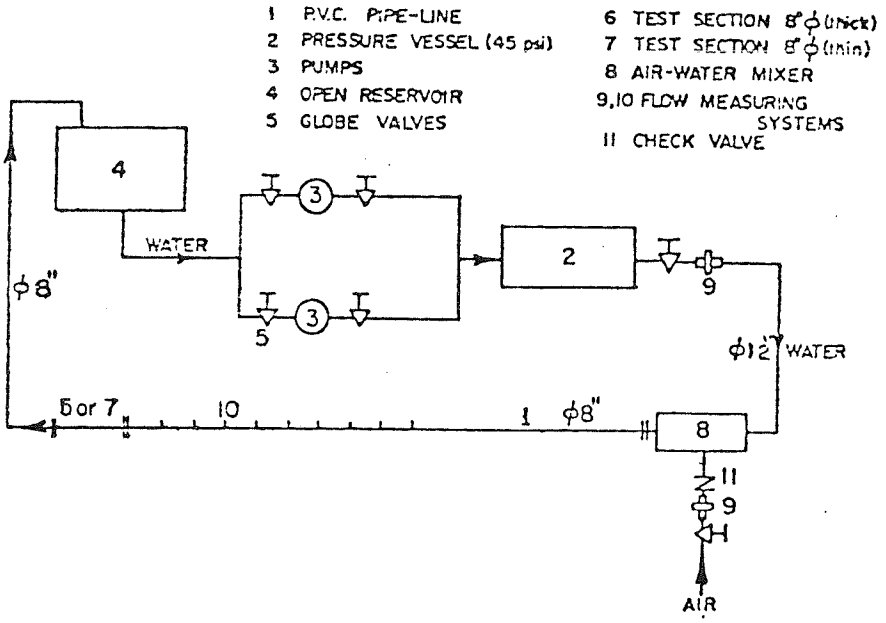

Figure 1 - Diagram of two-phase flow loop facility

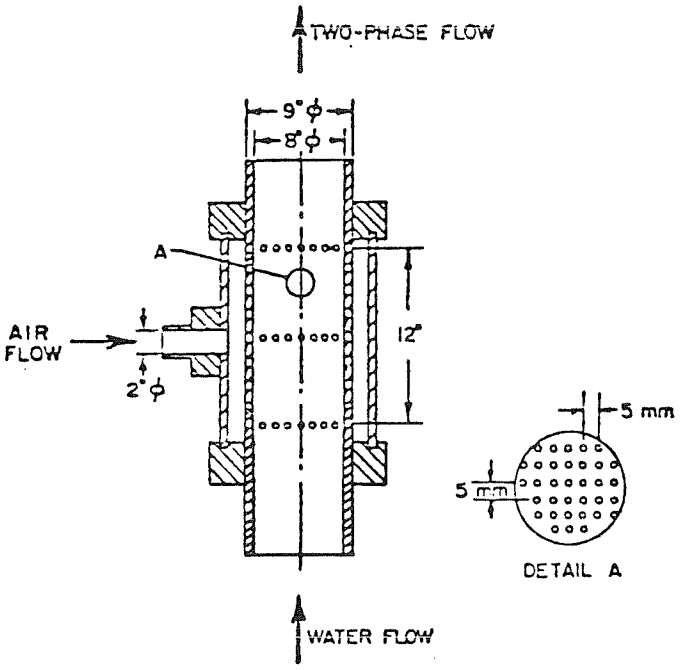

Figure 2 - Air-Water Mixture

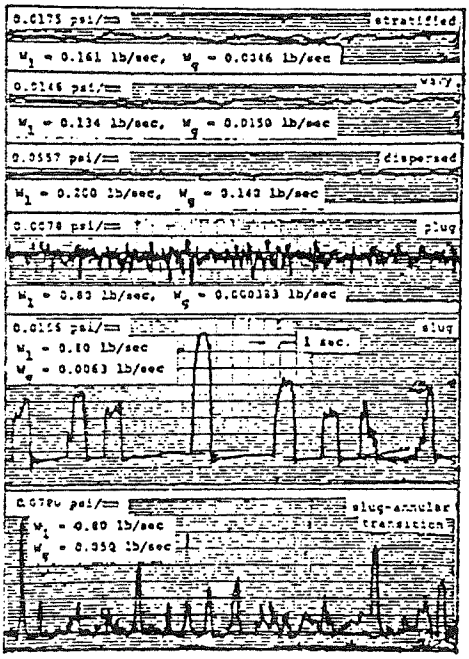

Figure 3 - Sample wall pressure traces for horizontal two-phase flow reproduced Hubbard and Dukler Ref. [7]

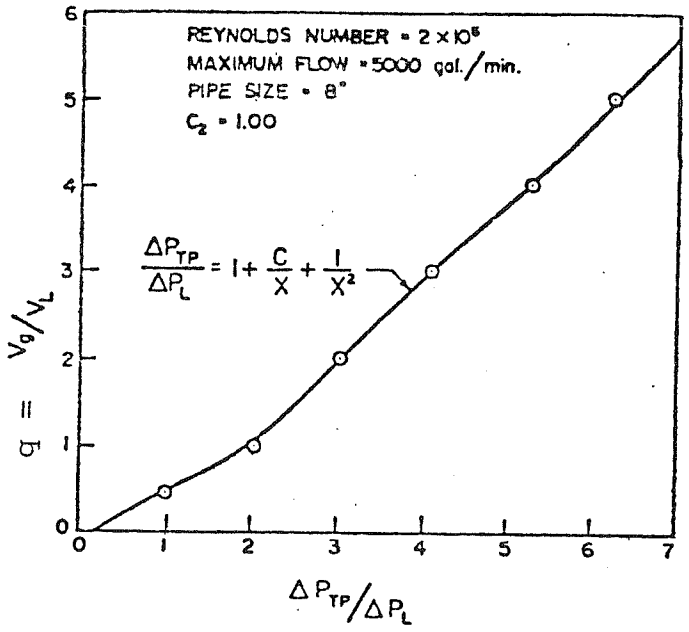

Figure 4 - Two-phase pressure drop versus mixture volumetric ratio, q

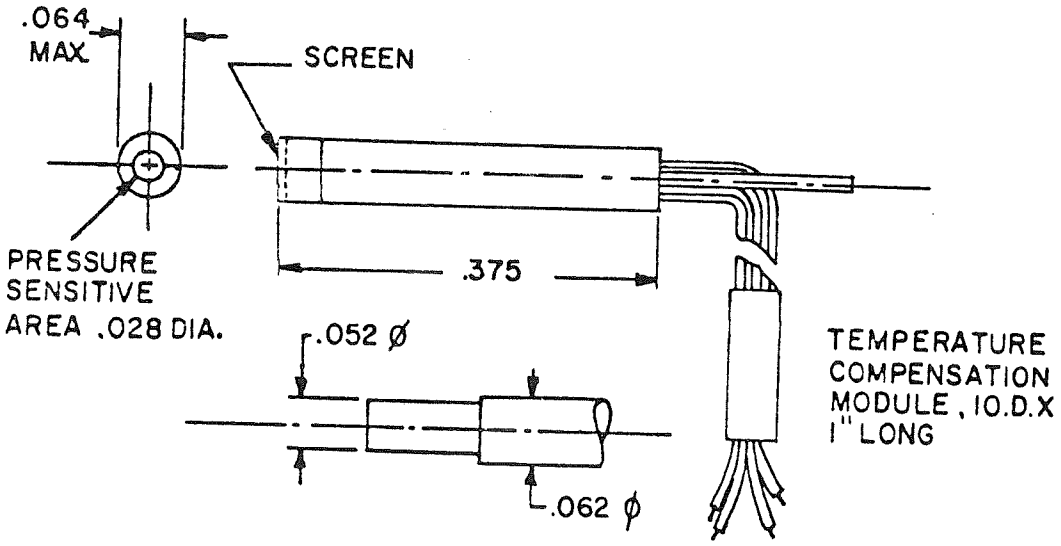

Figure 5 - Kulite pressure transducers series XQC-062

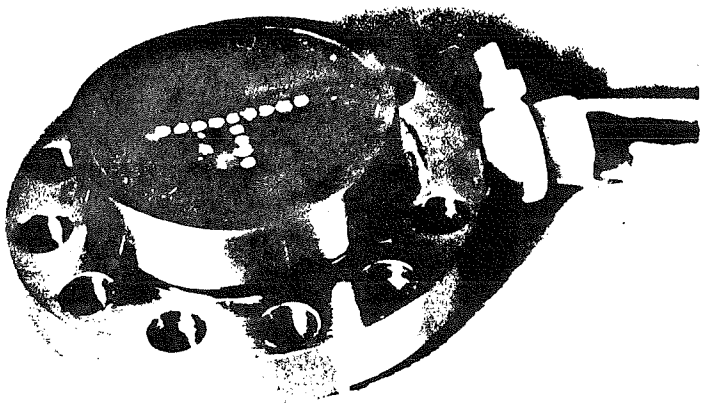

Figure 6 - T-slot, top view

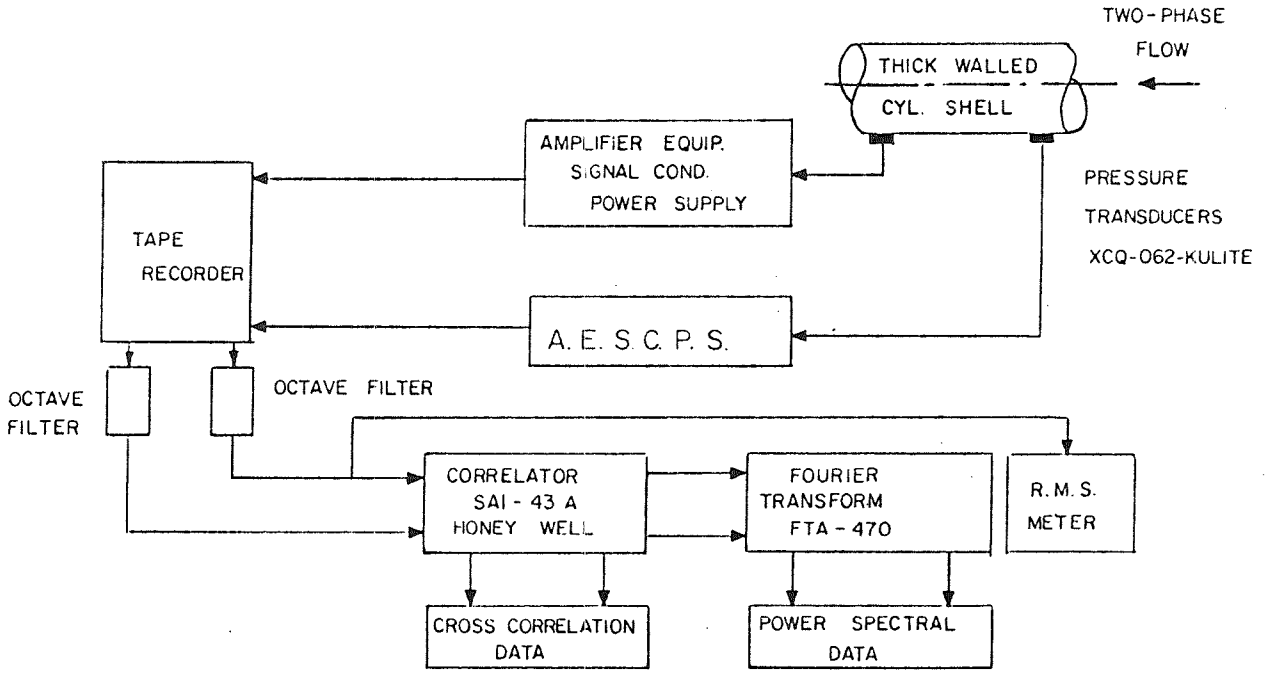

Figure 7 - Block diagram of instrumentation utilized for recording and analyzing turbulent wall pressure field

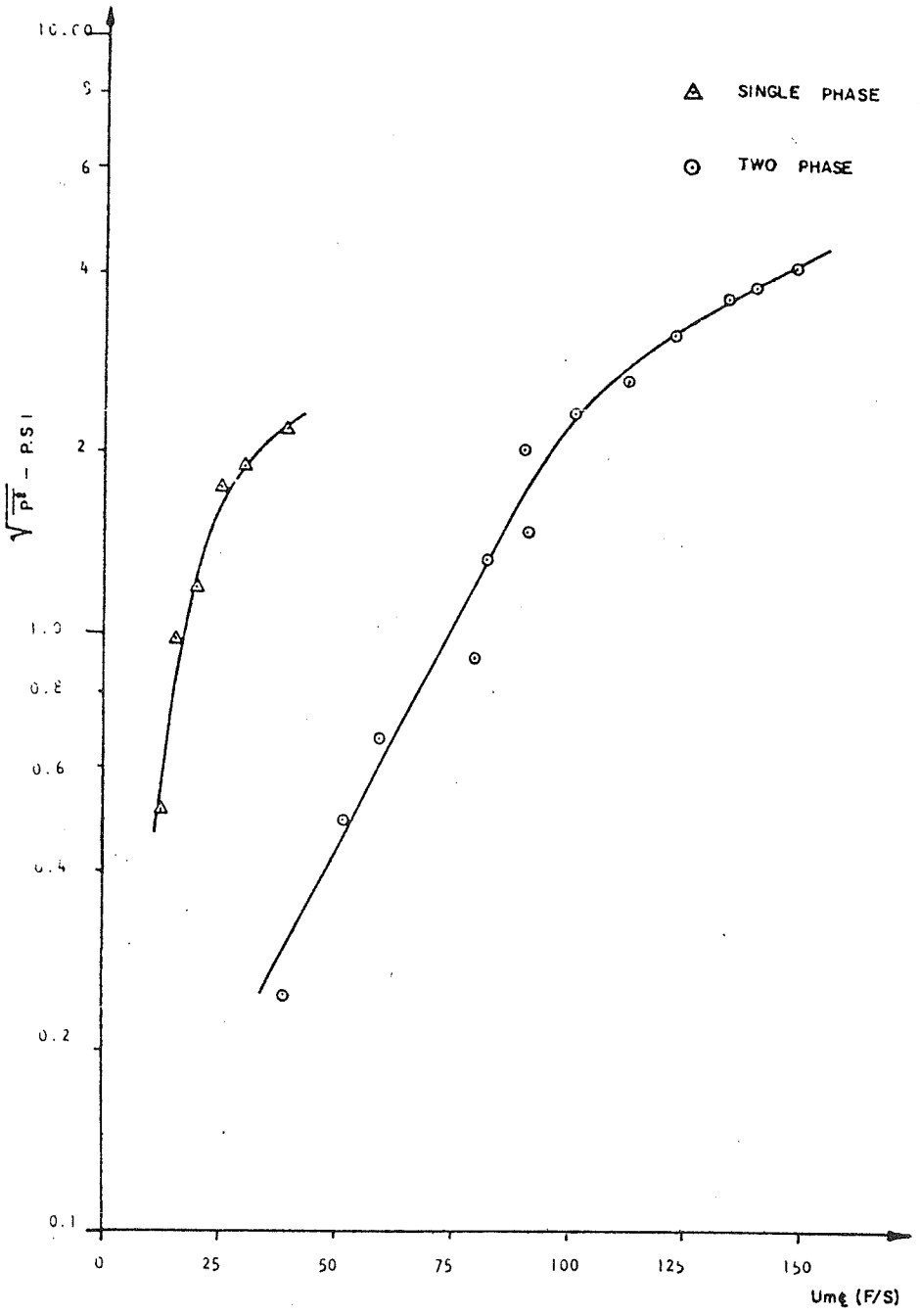

Figure 8 - Comparison between RMS, wall pressure fluctuation for single and two-phase versus mixture center-line velocity $U_{m\ell}$

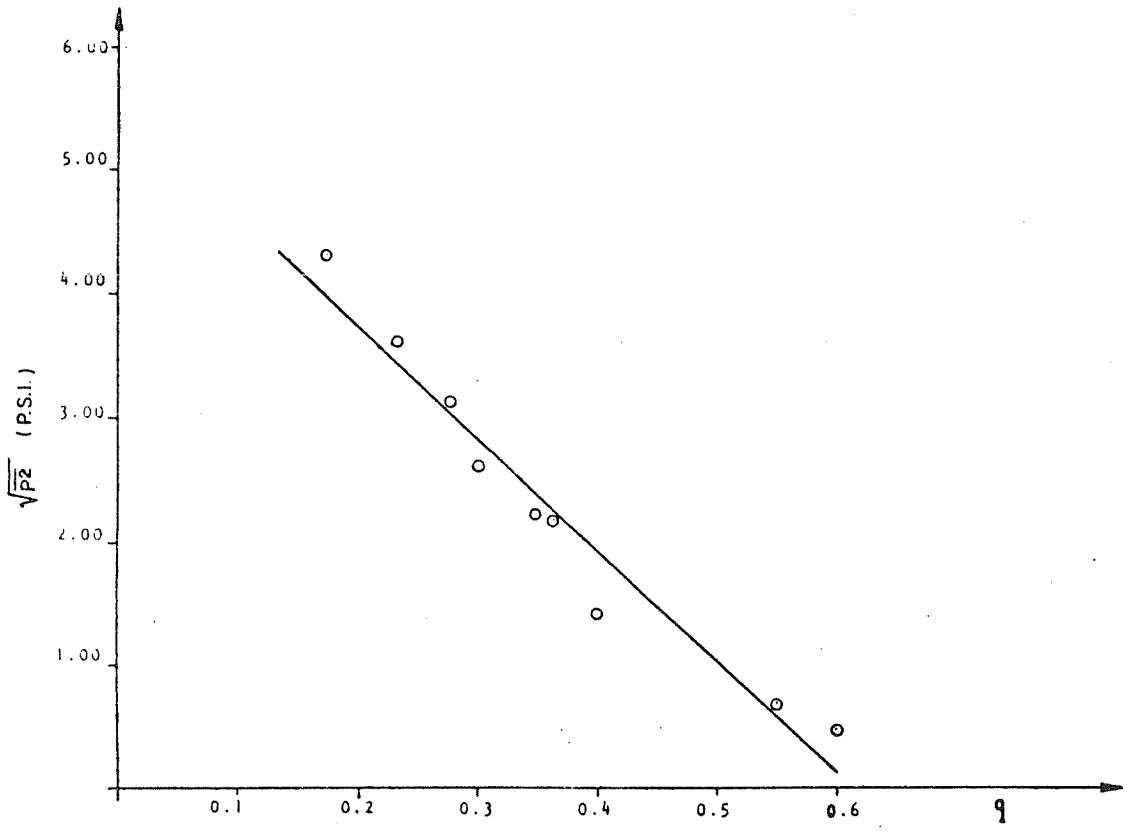

Figure 9 - RMS wall pressure, $\sqrt{\overline{P^2}}$, versus volumetric mixing ratio, q.

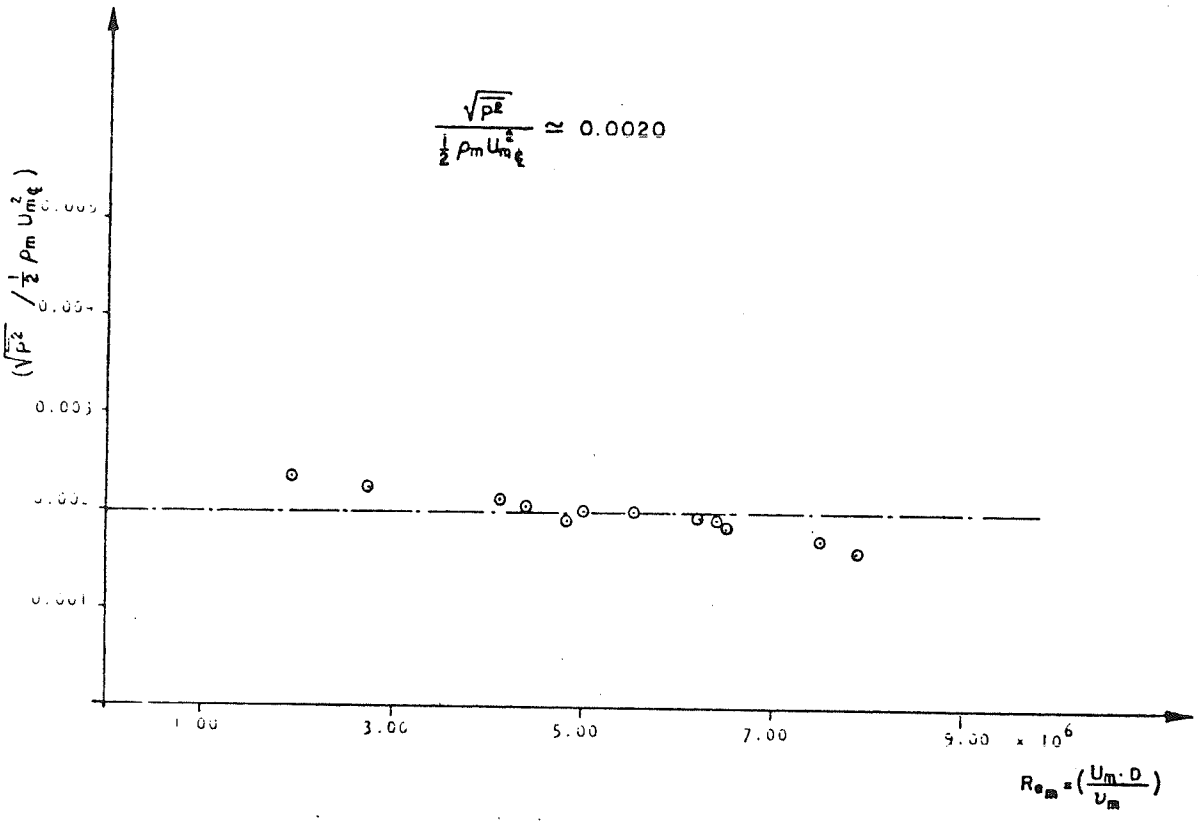

Figure 10 - Pressure Coefficient, $\frac{\sqrt{\overline{p^2}}}{1/2\ \rho_m\ U_{m_\ell}^2}$ versus Reynolds number, $\frac{U_m \cdot D}{\nu_m}$

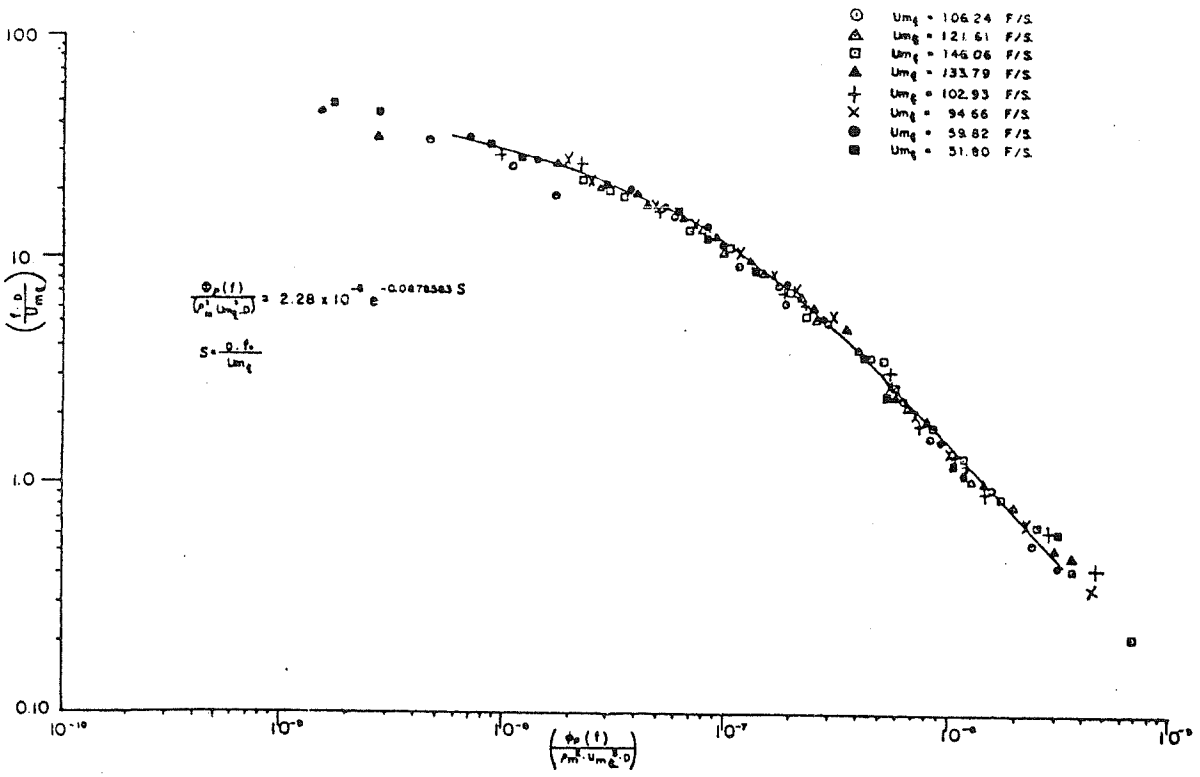

Figure 11 - Normalized power spectra, $\Phi_p(f)/\rho_m^2 U_{m\ell}^3 .D$ versus Strouhal Number, $S = \frac{f.D}{U_{m\ell}}$ for various mixture velocities, $U_{m\ell}$.

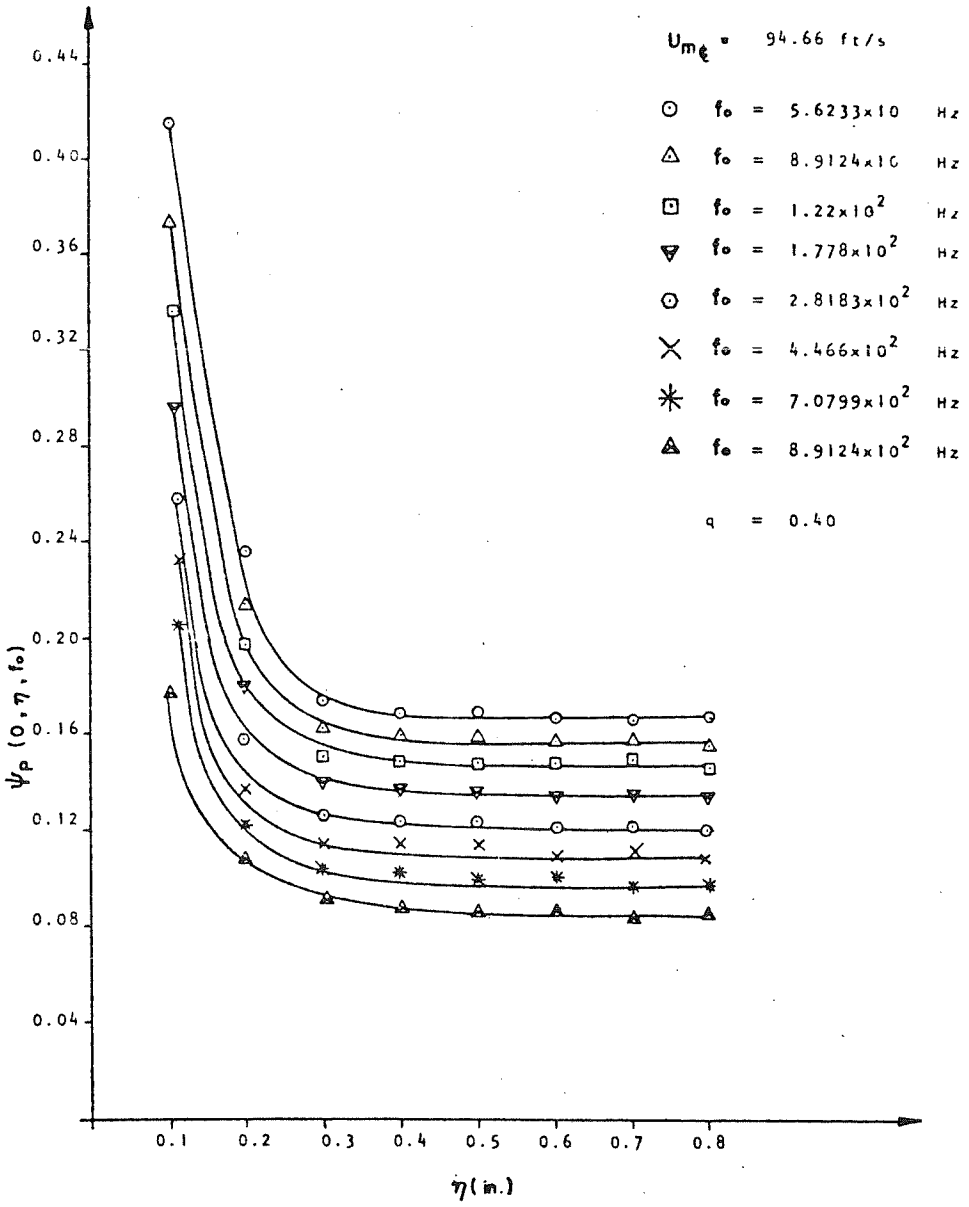

Figure 12 - Lateral pressure correlation, Ψ_p $(0,\eta,f_o 0)$ as a function of the transducers separation, η, for various center bands frequencies, f_o, and center-line mixture velocity, $U_{m_{\ell}}$ = 94.66 F/S.

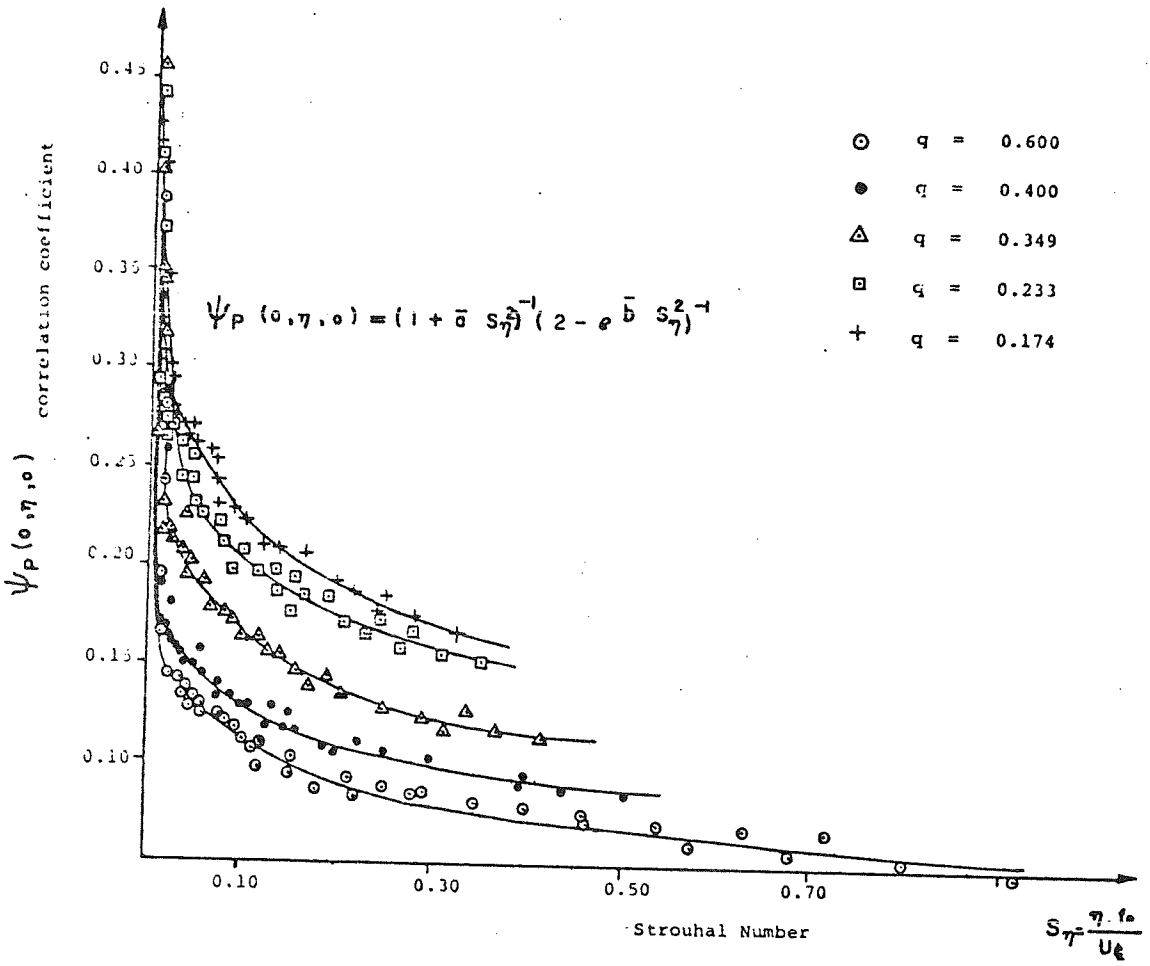

Figure 13 - Correlation coefficient in the lateral direction, $\Psi_p(0,\eta,0)$ as a function of frequency Number, S_n (Strouhal Number), for various volumetric mixing ratio, q.

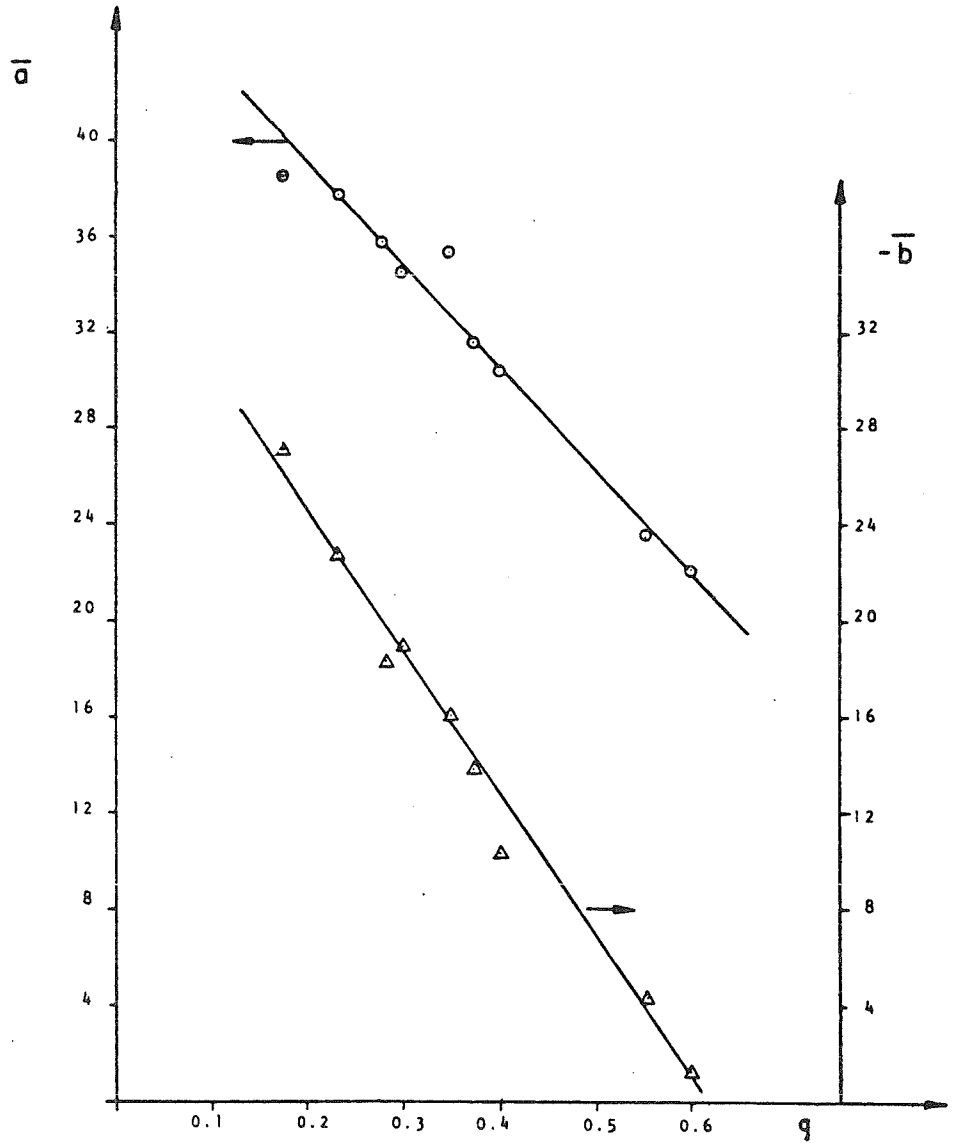

Figure 14 - Variable $\bar{a}$ and $\bar{b}$, as a function of volumetric mixing ratio, q

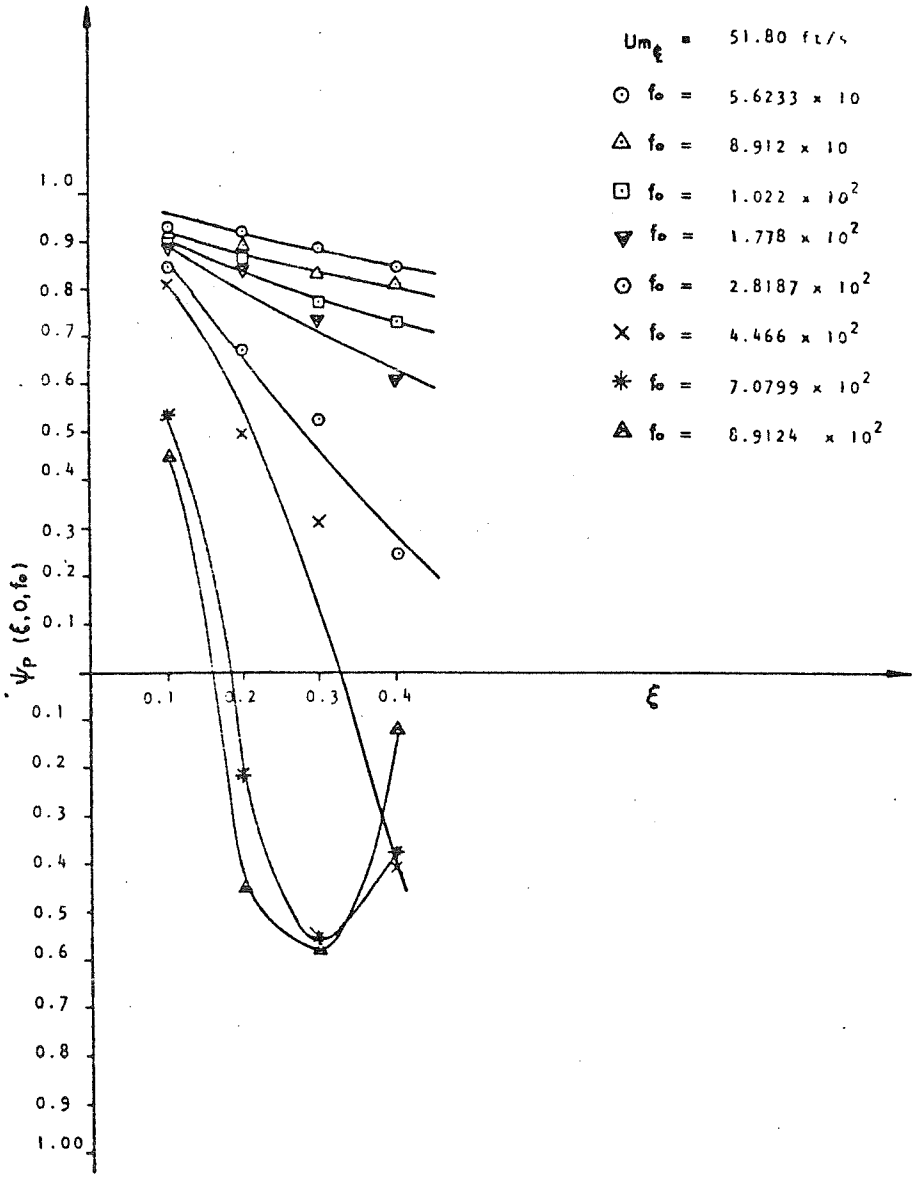

Figure 15 - Axial correlation, $\Psi_p(\xi,0,f_o)$ versus axial separation, ξ, (in,) for various center band frequencies, f_o, at center-line velocity, $U_{m_{CL}}$ = 51.80 F/S.

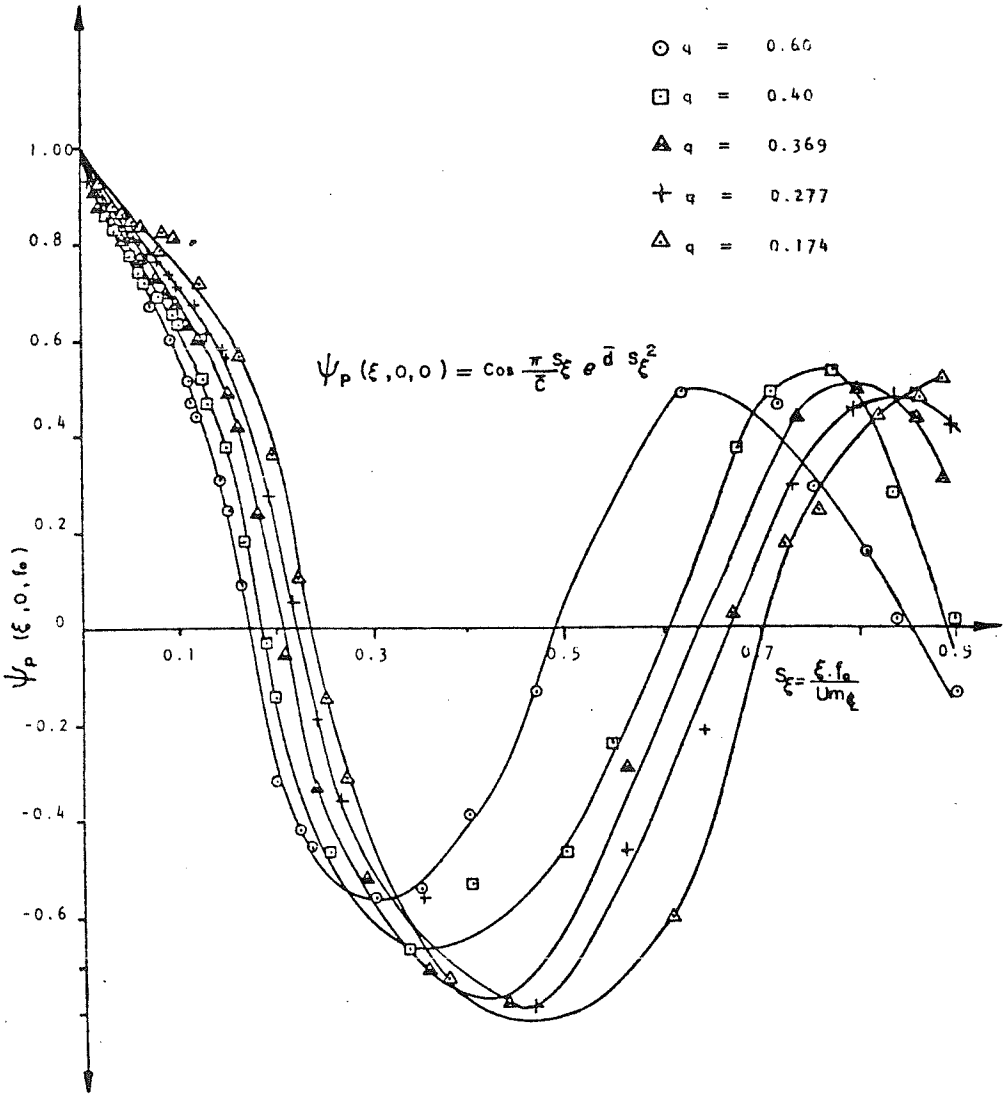

FIGURE 16 - Axial correlation coefficient, ψ_p (ξ,o,o) as a function of Strouhal Number, $S\xi$, for various volumetric mixing ratio, q.

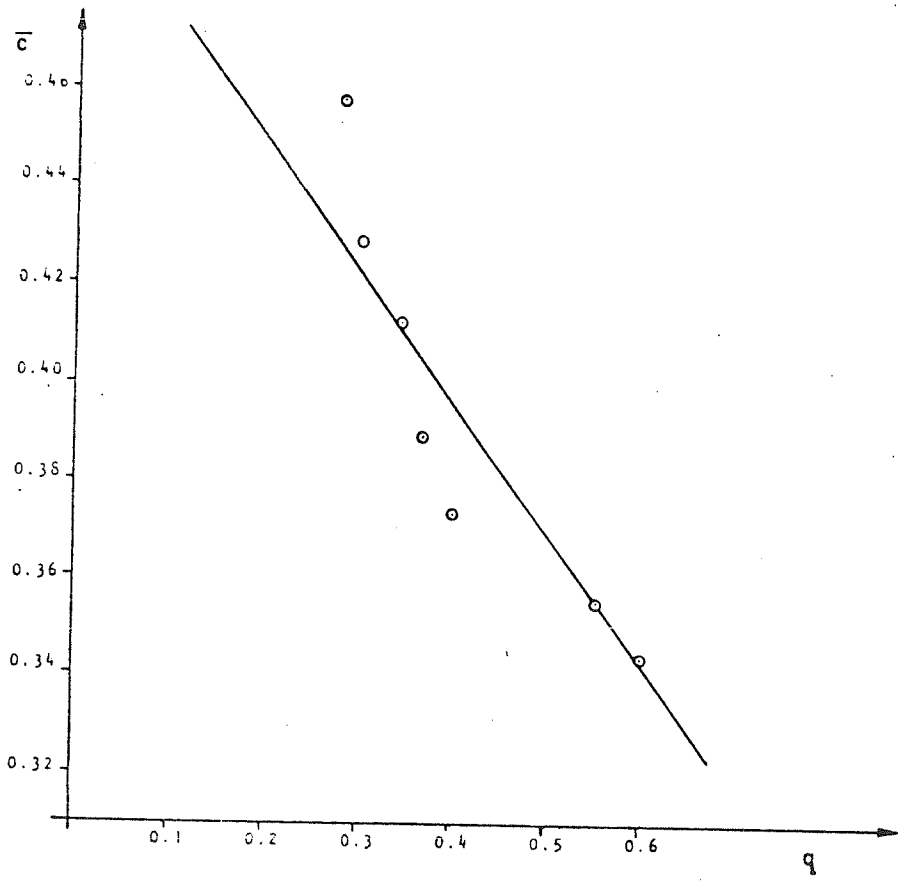

Figure 17 - Parameter $\bar{C}$ as a function of volumetric mixing ratio, q

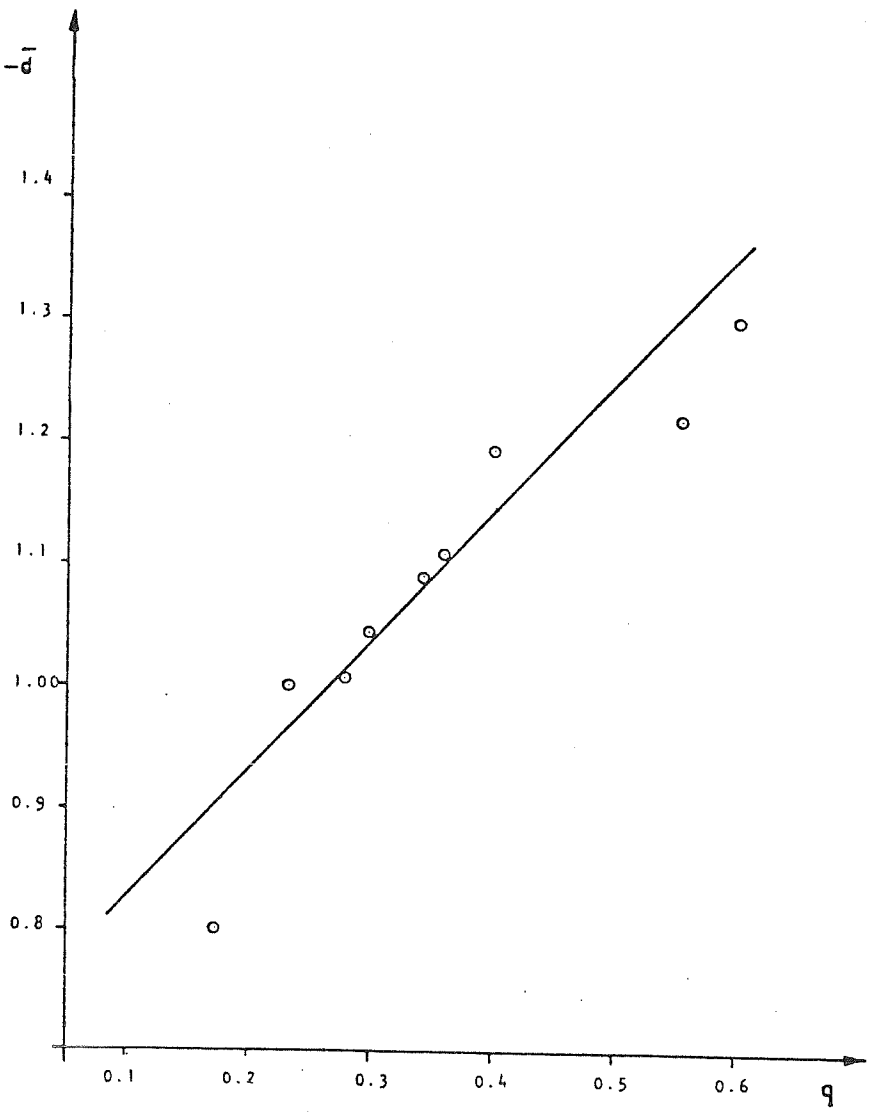

Figure 18 - Parameter $\bar{d}$ as a function of volumetric mixing ratio, q

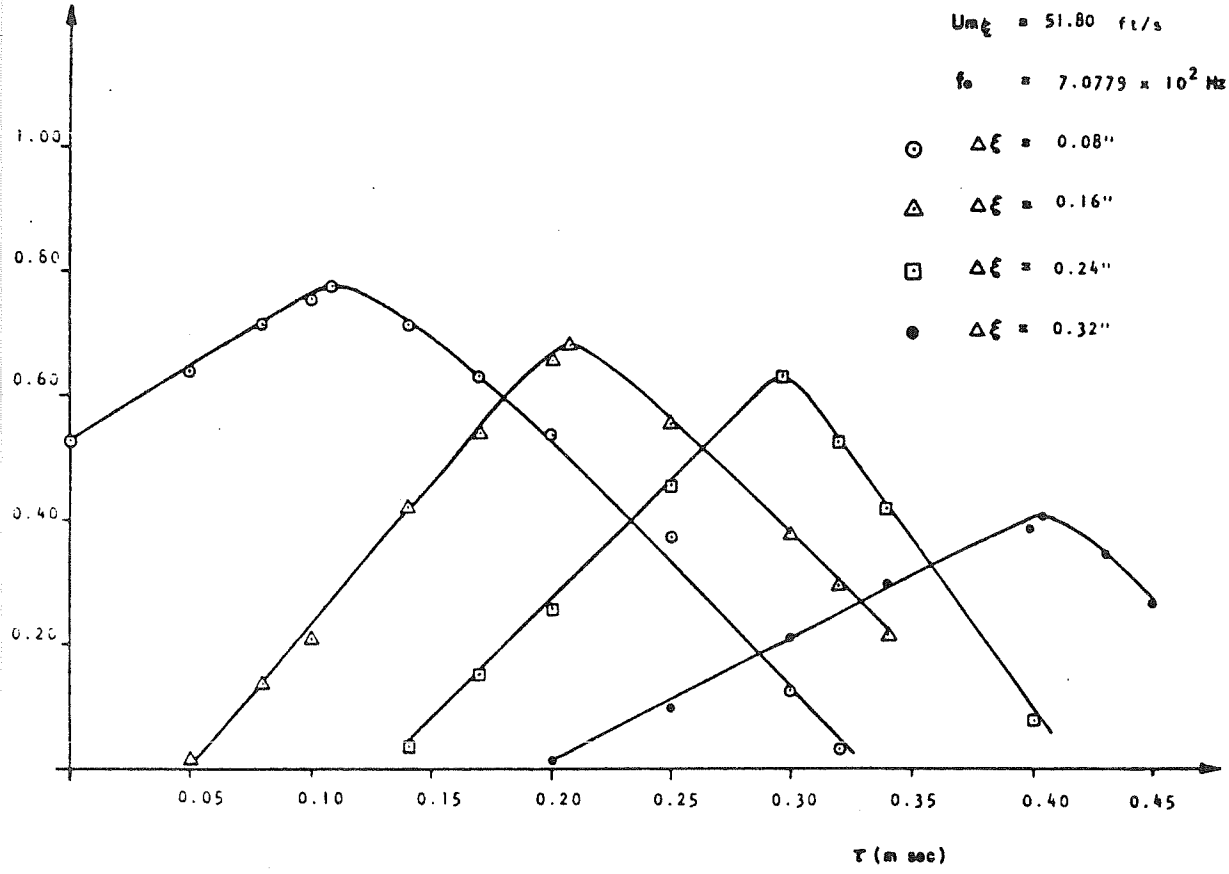

FIGURE 19 - Correlation coefficient, $\psi_p(\xi,0.\tau)$, versus time delay, τ, at center line mixture velocity, $U_{m\mathcal{L}}$ and center band frequency, f_o.

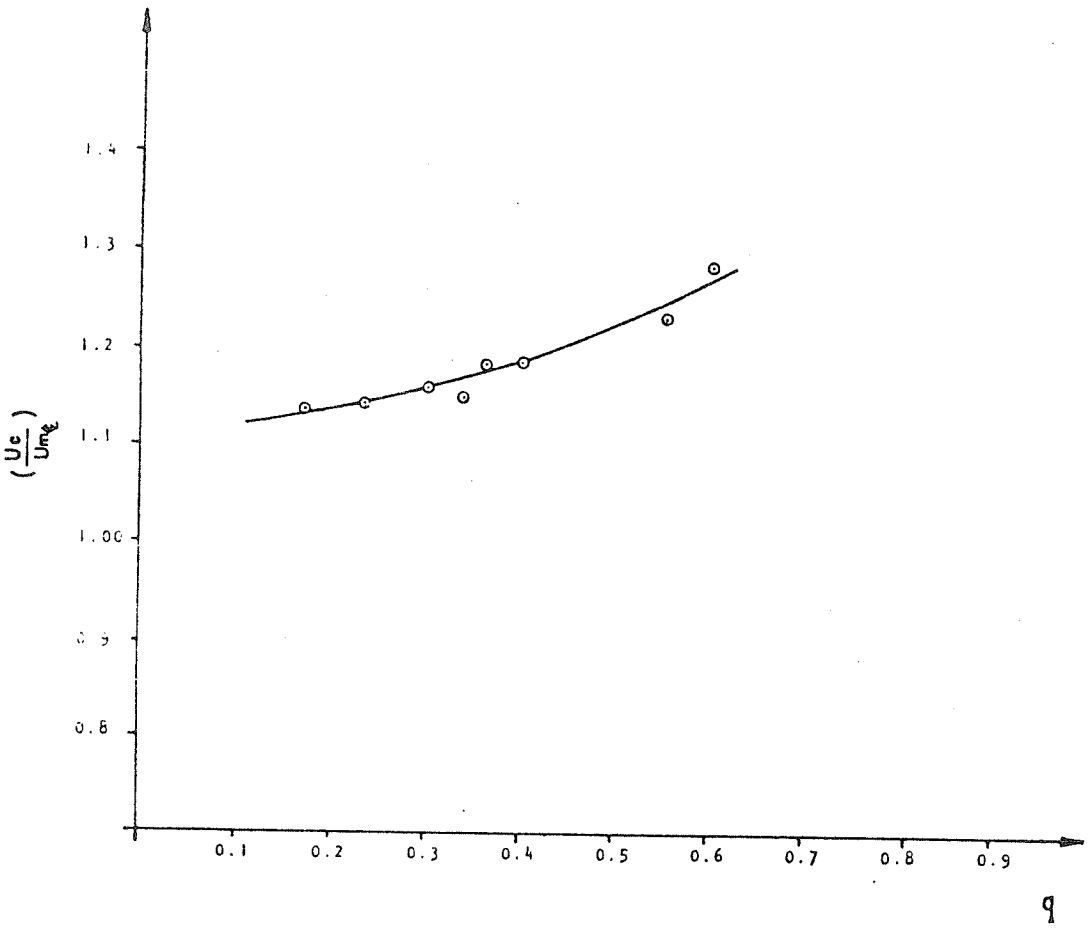

FIGURE 20 - Normalized convection velocity, $\frac{U_c}{U_{m\ell}}$ as a function of the volumetric mixing ratio, q.

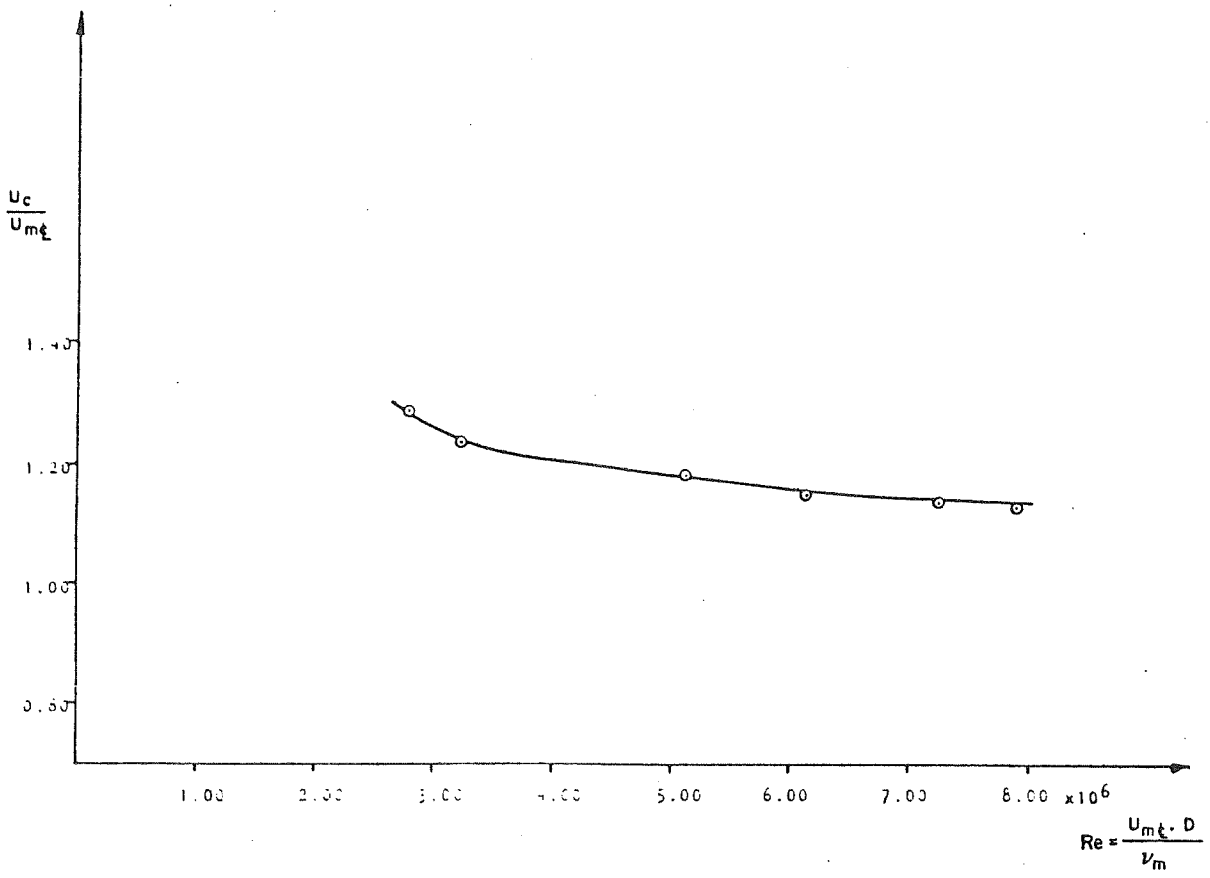

FIGURE 21 - Normalized convection velocity $\frac{U_c}{U_{m_\ell}}$ as a function of Reynold's number, $Re = \frac{U_{m_\ell} \cdot D}{\nu_m}$

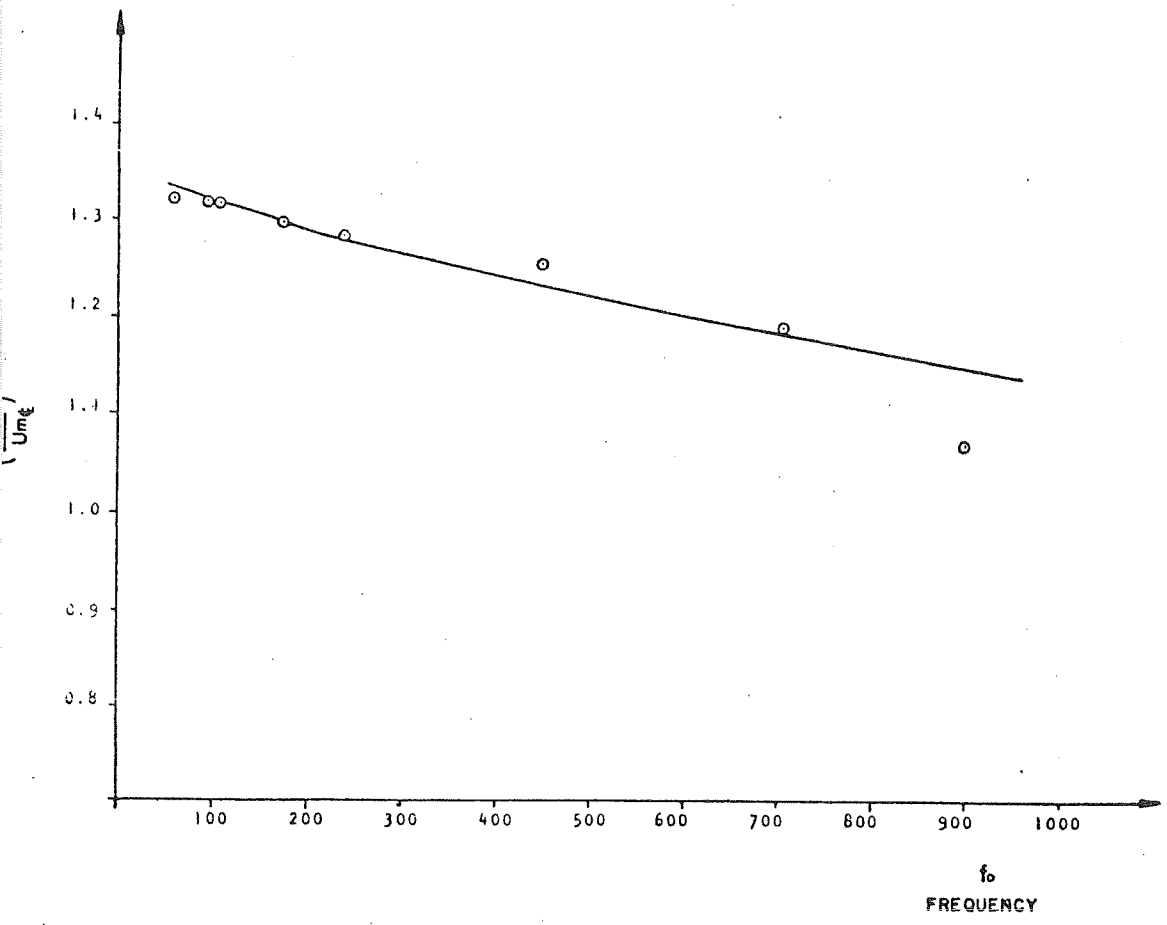

FIGURE 22 - Normalized convection velocity, $\frac{U_c}{U_{m_{\mathcal{L}}}}$ as a function of the center-band frequency, f_o.

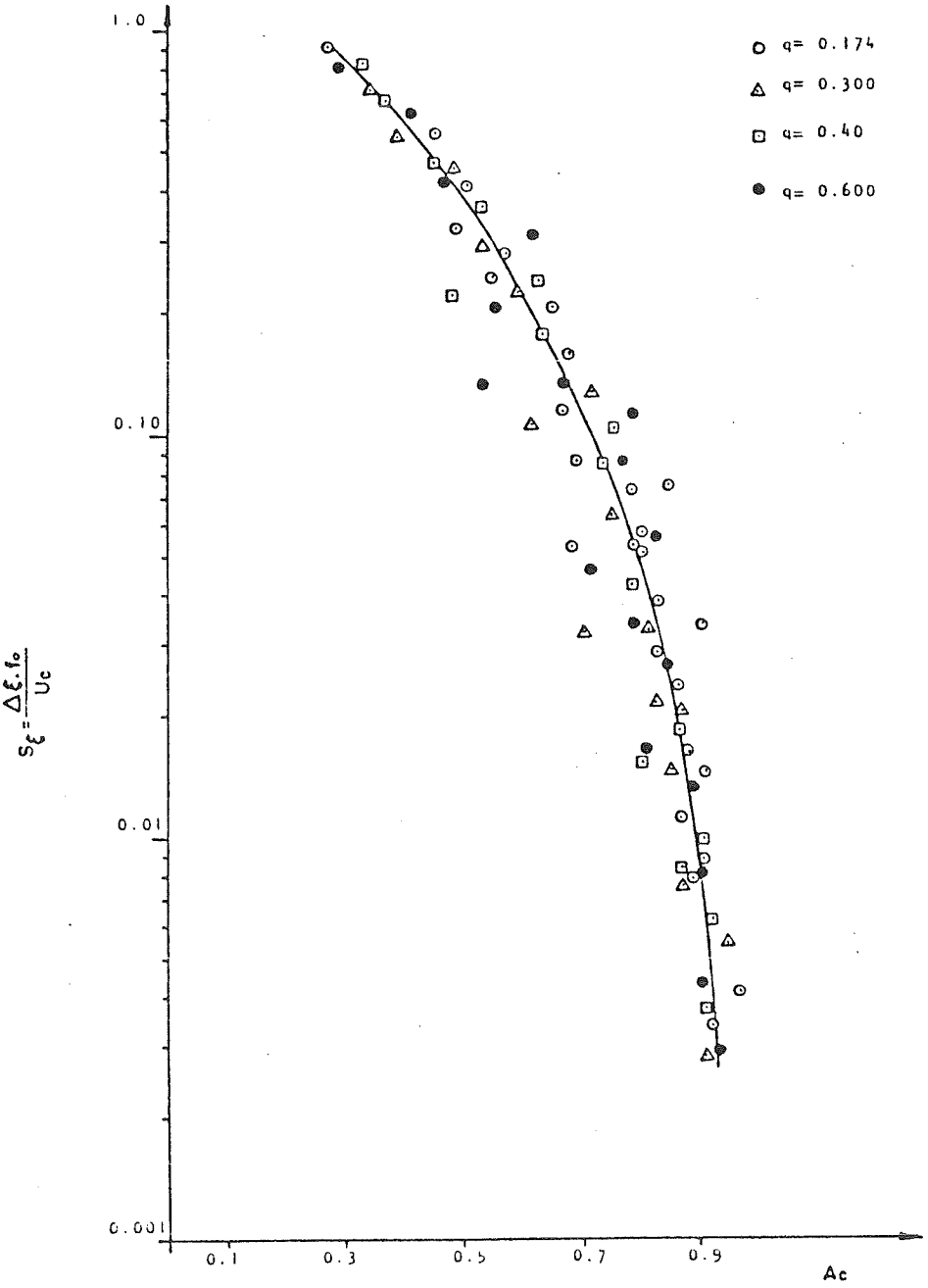

FIGURE 23 - The amplitude of the normalized correlation coefficient, Ac, as a function of the axial Strouhal Number, $S_\xi = \frac{\Delta\xi . fo}{U}$, on convection velocity, Uc, basis, at various mixing ratios, q.

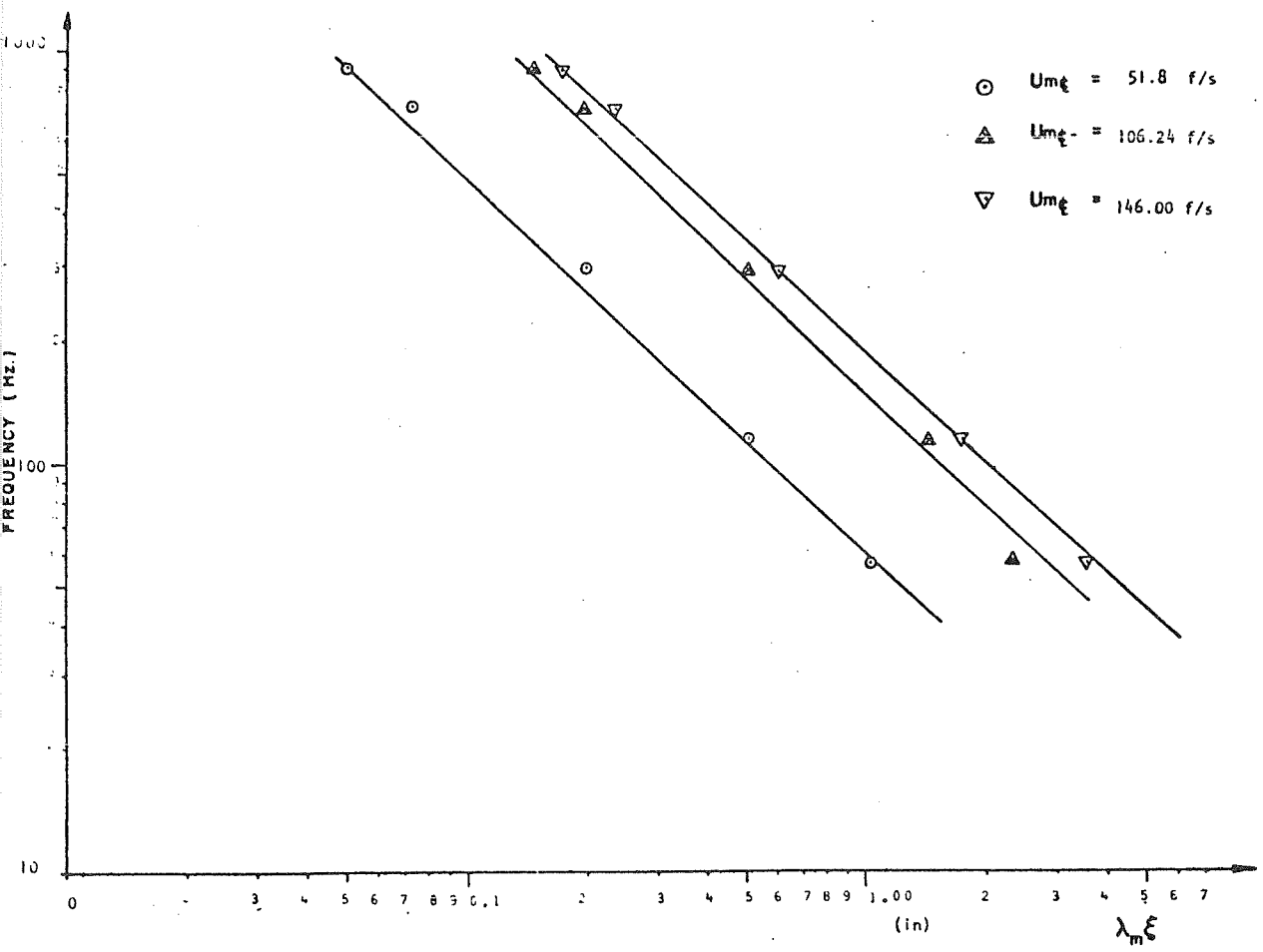

FIGURE 24 - Axial microscale, $\lambda_{m\xi}$,
versus center band frequency for
various mixture center-line velocity , $U_{m\xi}$

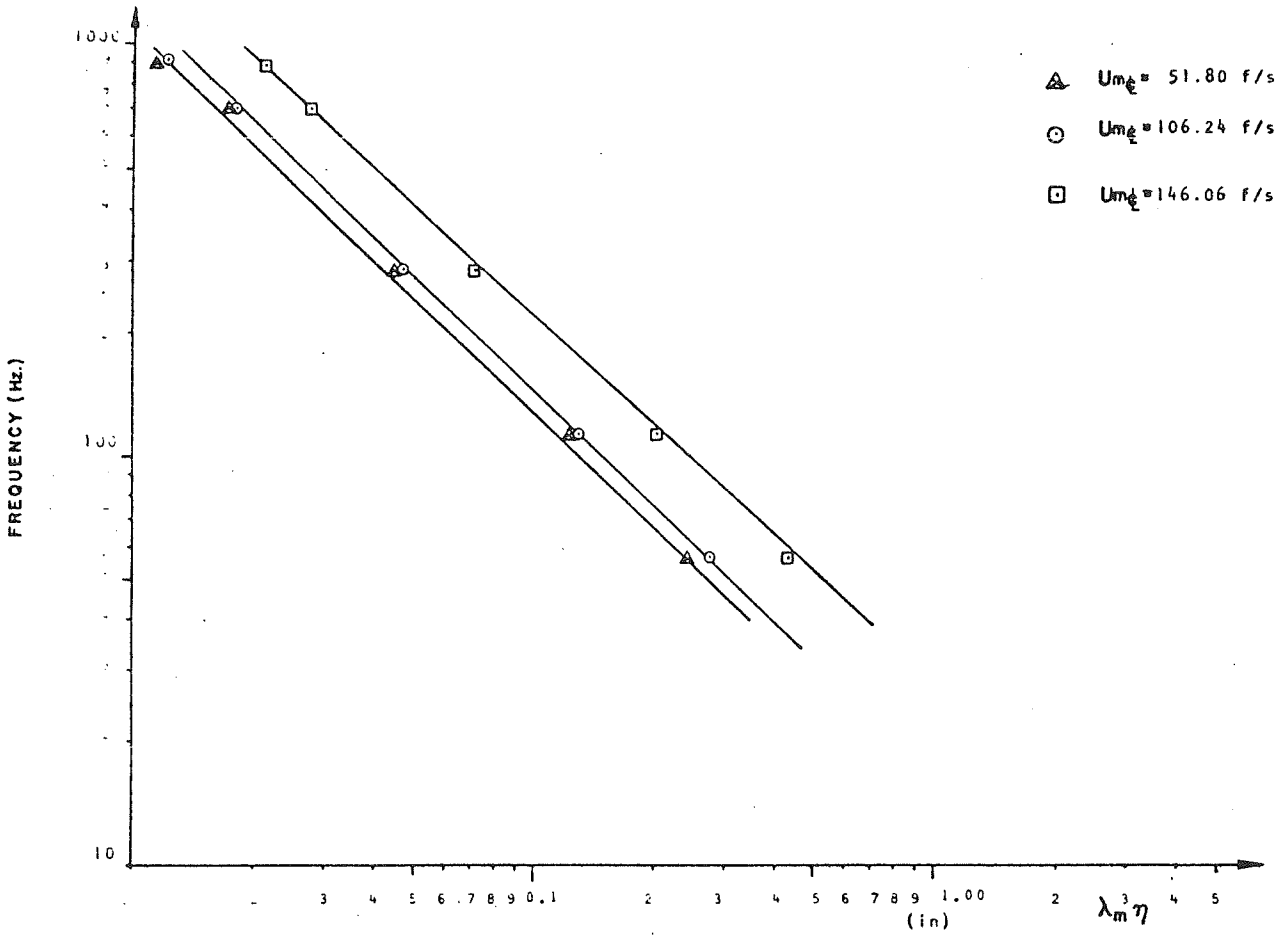

FIGURE 25 - Lateral microscale, $\lambda_{m\eta}$, as a function of the center band frequency for different mixture center line velocity, $U_{m\ell}$.

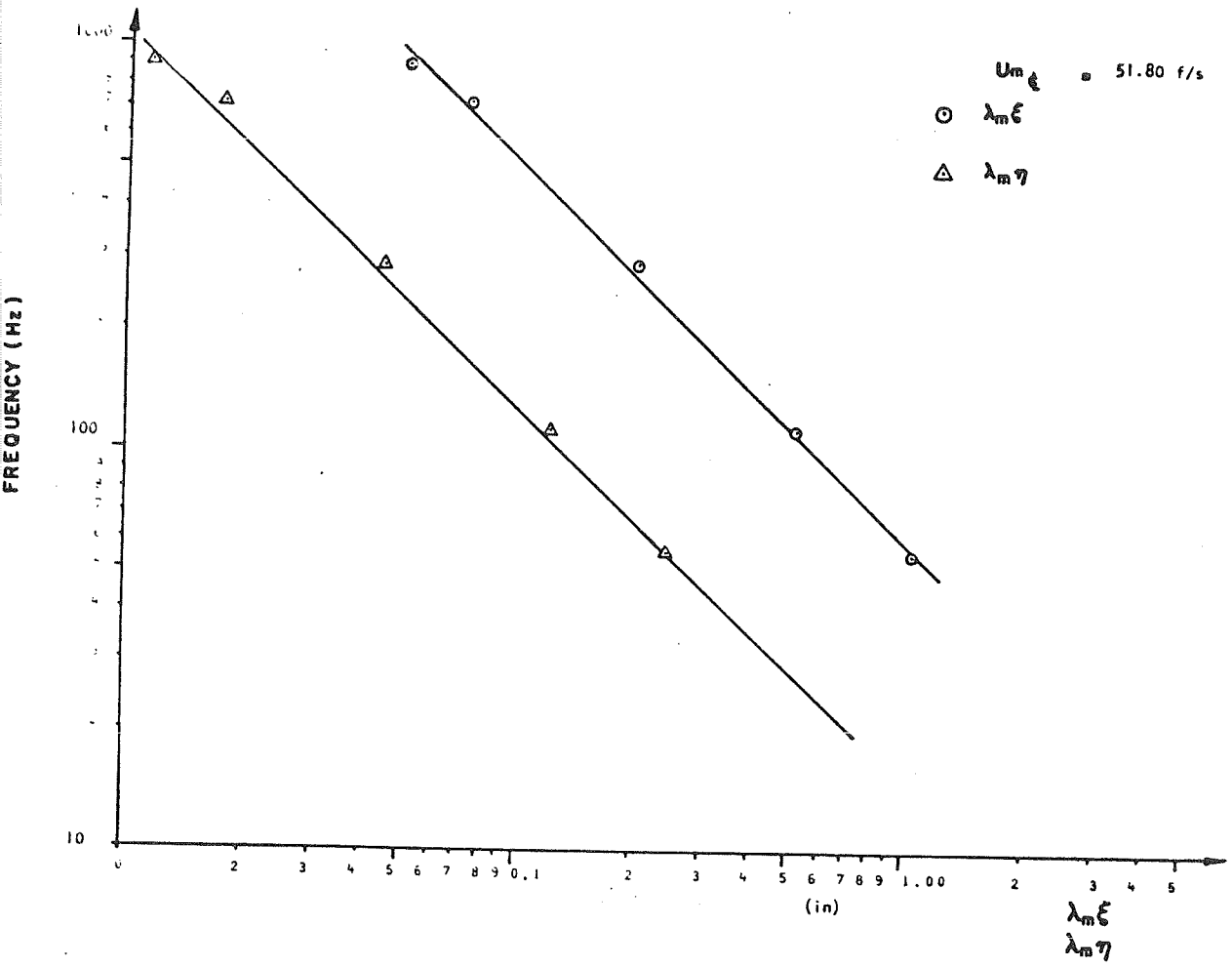

FIGURE 26 - Axial and lateral microscales, $\lambda_{m\xi}$, and, $\lambda_{m\eta}$ respectively as a function of the center band frequency for mixture center-line velocity, $U_{m\mathcal{L}}$ = 51.80 F/S.

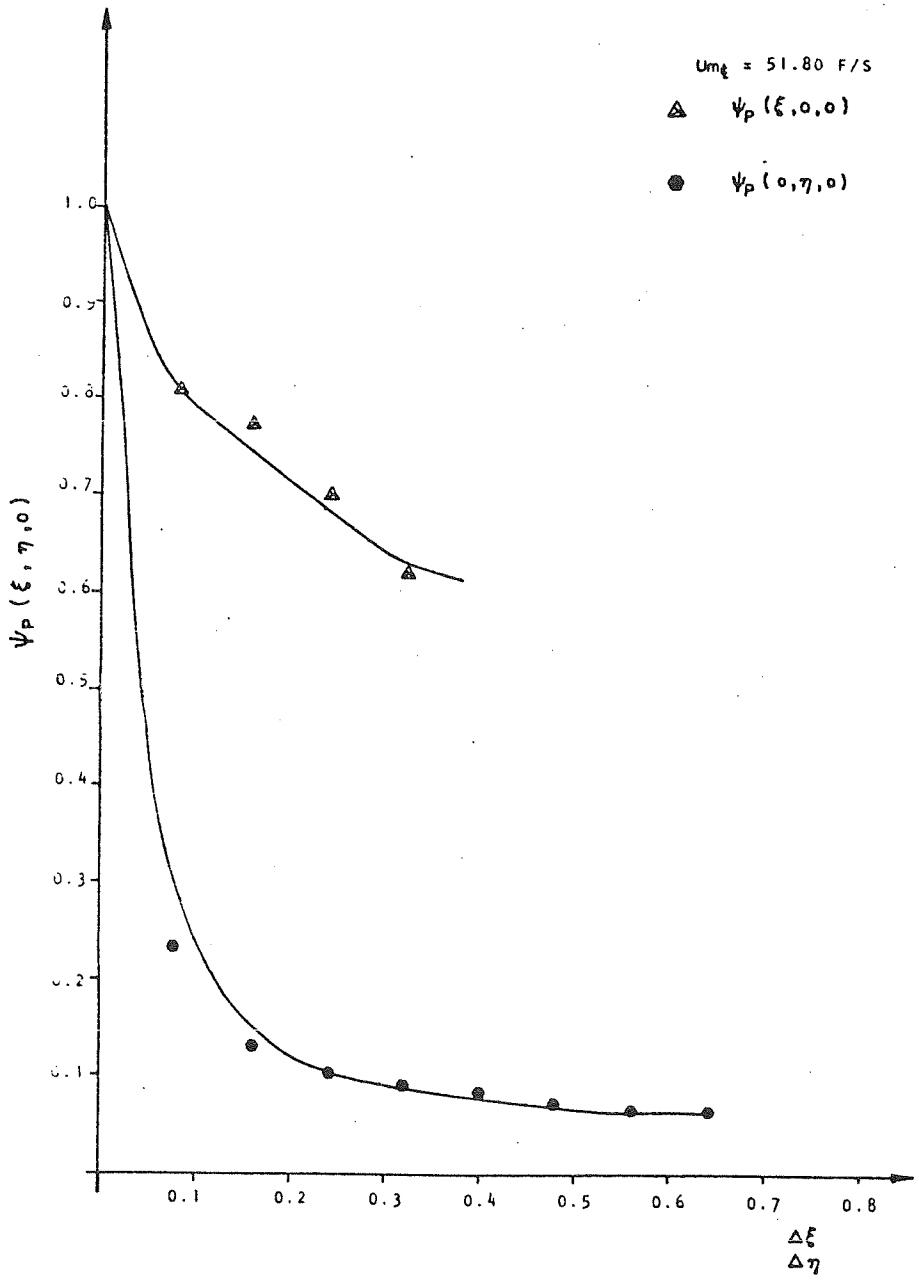

FIGURE 27 - Broad band correlation coefficient, $\psi_p(\xi,\eta,o)$ versus axial and lateral transducer, separations, $\Delta\xi$, $\Delta\eta$, respectively at volumetric mixing ratio, q = 0.60.

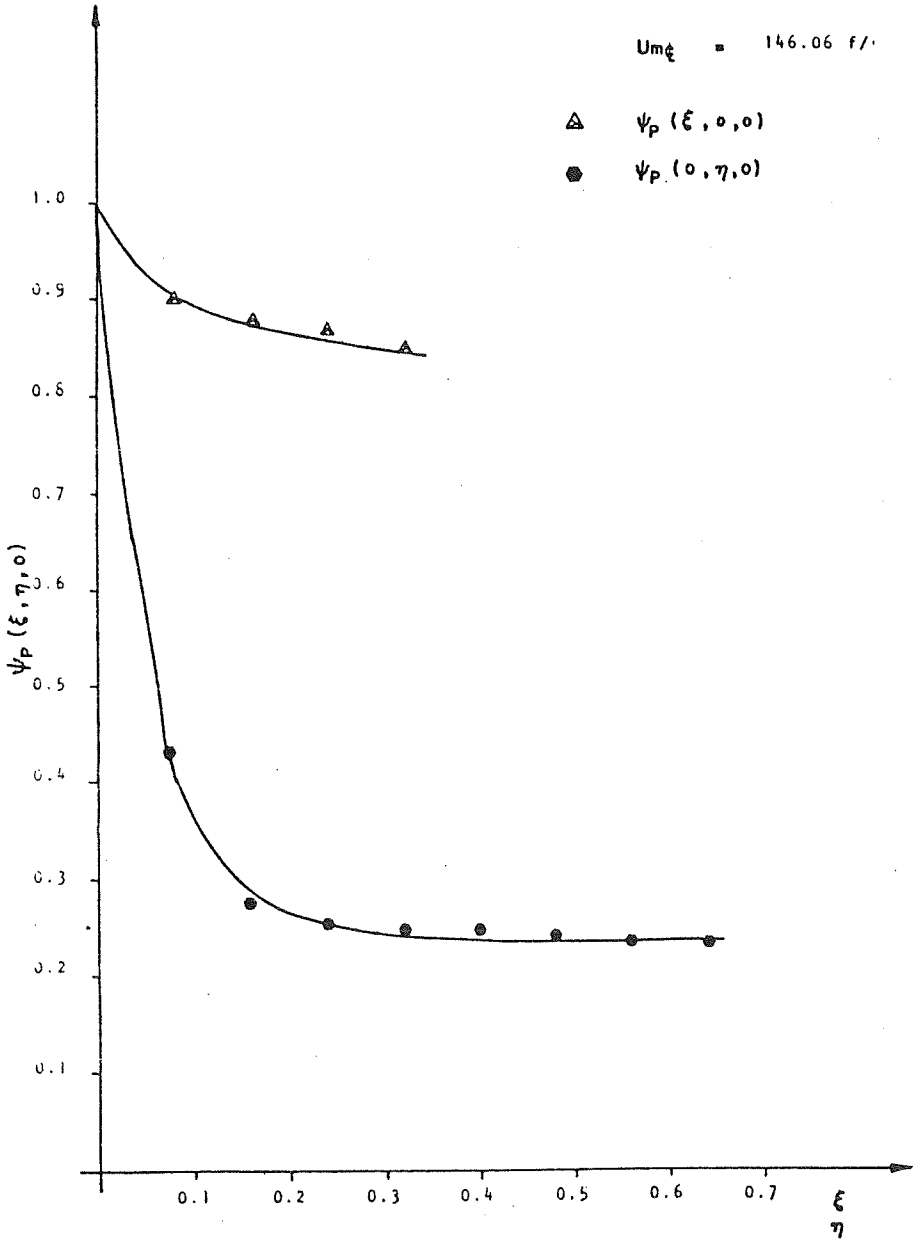

FIGURE 28 - Broad band correlation, $\psi_p(\xi, \eta, o)$, versus axial and lateral separation, ξ, and, η, respectively at center-line mixture velocity, $U_{m\ell}$ = 146.06 F/S.

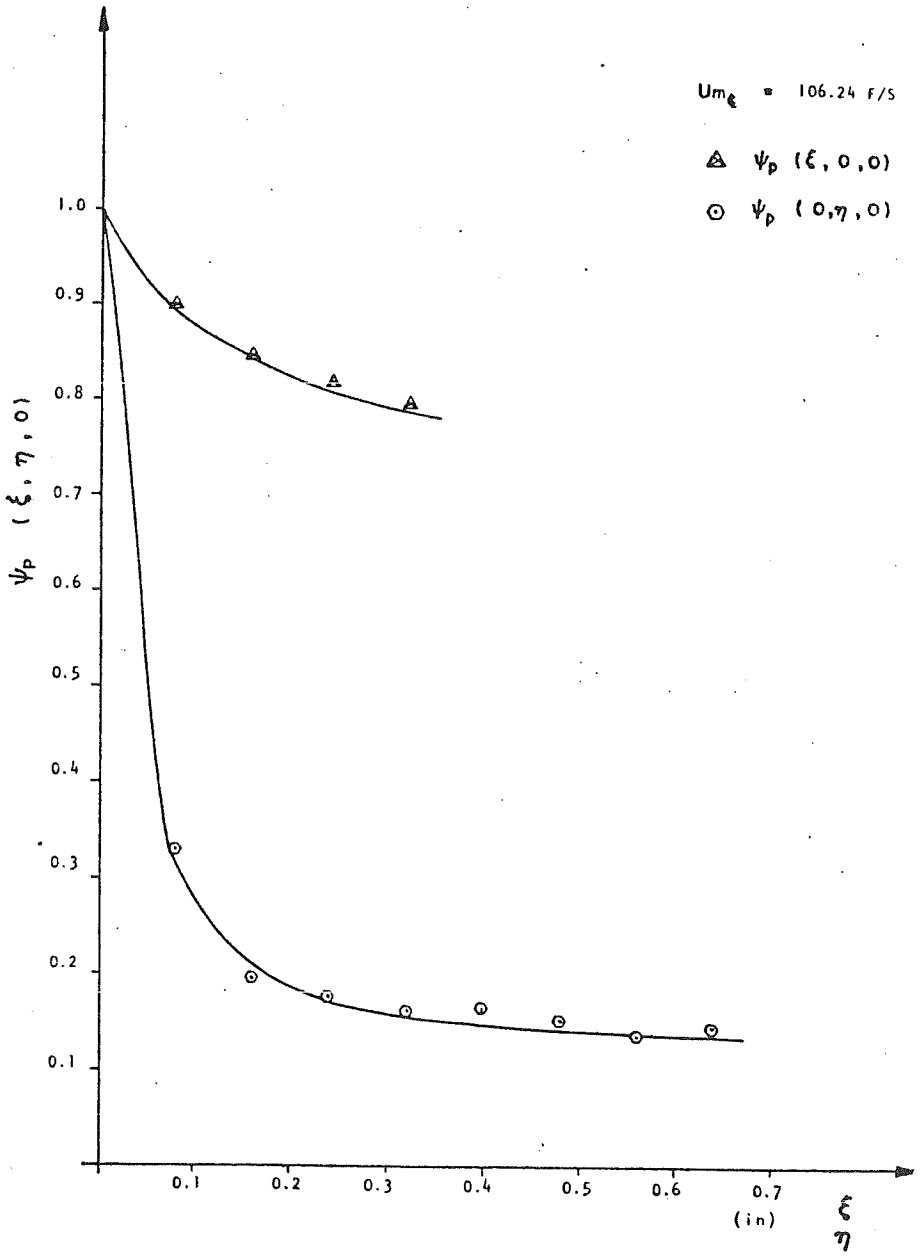

FIGURE 29 - Broad band correlation coefficient, $\psi_p(\xi, \eta, o)$ versus transducer separation, ξ, η, in the axial and lateral direction respectively at center line mixture velocity, $U_{m\mathbb{C}}$ = 106.24 F/S.

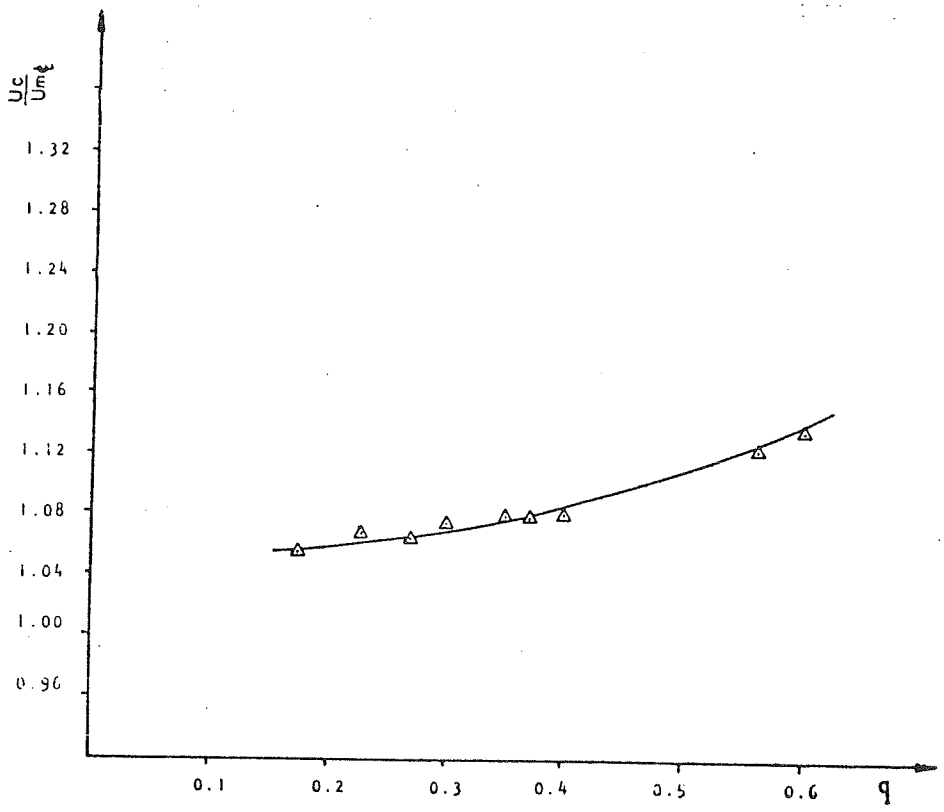

FIGURE 30 - Broad band convection velocity ratio, $\frac{U_c}{U_{m\mathbb{C}}}$ versus volumetric mixing ratio, q